Artificial Intelligence in Geosciences 7 (2026) 100202

Contents lists available at ScienceDirect

Artificial Intelligence in Geosciences

journal homepage: www.keaipublishing.com/en/journals/artificial-intelligence-in-geosciences

Unlocking the potential of legacy data for future geoenergy and storage applications: Porosity and permeability prediction based on machine learning applied to petrographic data

Benjamin Busch *, Christoph Hilgers

Structural Geology and Tectonics, Institute of Applied Geosciences, Karlsruhe Institute of Technology, Adenauerring 20a, 76131, Karlsruhe, Germany

ARTICLE INFO

Keywords:
Machine learning
Petrography
Point-counting
Porosity
Permeability
Reservoir quality

ABSTRACT

Machine learning techniques are increasingly applied in geological research and widely adopted in industry. However, one commonly available dataset remains underutilized: petrographic data from classical point-counting analyses. These data, routinely collected for reservoir lithologies worldwide, are often paired with core measurements such as porosity and permeability and capture detrital and authigenic components, textural properties, and diagenetic effects that largely govern reservoir quality.

Building on an initial proof of concept, we expand the scope to a legacy dataset comprising 875 samples from 51 wells, compiled over 25 years by at least 21 petrographers. This dataset demonstrates the feasibility of predicting porosity and permeability from point-counting data across diverse lithologies and sources. Despite potential operator bias and classification inconsistencies, predictive performance remains robust.

We present the outcome from two Histogram-based Gradient Boosting Regression Tree models trained on four major reservoir lithologies in Germany and the Netherlands: Upper Carboniferous, Permian Rotliegendes, Triassic Buntsandstein, and Jurassic sandstones. The porosity model achieves $R^2 = 0.87$, MAE = 1.77%, and RMSE = 2.23%. The permeability model (log-transformed) yields $R^2 = 0.82$, MAE = 0.47, and RMSE = 0.64, consistent with the log-normal distribution of permeability. SHAP analyses highlight key petrographic features influencing predictions, offering insights into detrital and diagenetic reservoir quality controls.

Model performance remains robust under well-wise splits, confirming applicability to unseen wells. Training on cored intervals may enable extension to cuttings, which are more continuously available along well sections. Leveraging such legacy datasets can enhance reservoir quality assessment in sample-limited projects and improve the understanding of global reservoir systems.

1. Introduction

In recent years, machine learning has been extensively applied to subsurface geology (Bergen et al., 2019; Karpatne et al., 2019; Dramsch, 2020), with use cases ranging from well log analysis and rock property estimation (Mishra et al., 2022; Ore and Gao, 2023; Joshua et al., 2024; Chen et al., 2025; Soromotin et al., 2025), drilling optimization (Shi et al., 2025), reservoir engineering (Sinha and Dindoruk, 2025), field development (Du et al., 2025; Guo and Sankaran, 2025), pore classification (Yang et al., 2025), porosity and permeability evaluation during drilling (Sun et al., 2021), rock description (Dalhat and Osman, 2025), seismic interpretation (Wrona et al., 2018), CO_2 sequestration (Abdulkhaleq et al., 2025), to facies classification (Dubois et al., 2007; Duarte et al., 2023).

Reservoir-relevant properties like porosity and lithology can be derived from well logs using machine learning and are already in use (Wood, 2020). The largest number of machine learning applications focus on the utilization of well log data and well log-based classification of reservoir facies or lithotypes, as well logs are commonly available along longer well sections and are already computer digestible in digital formats or readily digitized. However, diagenetic factors influencing reservoir quality remain underexplored, mainly due to the limitations of geophysical logs, which only partially reflect specific mineral phases. As a result, understanding diagenetic controls on reservoir quality still

Peer review under the responsibility of KeAi Communications Co., Ltd.
* Corresponding author.
E-mail address: benjamin.busch@kit.edu (B. Busch).

https://doi.org/10.1016/j.aiig.2026.100202
Received 19 December 2025; Received in revised form 2 February 2026; Accepted 9 March 2026
Available online 10 March 2026

requires integrating petrographic and petrophysical data.

Machine learning is being used to analyze petrographic samples, extracting mineral composition, porosity distribution, capillary pressure curves, petrofacies relationships, and to describe rock types (Rubo et al., 2019; Tang et al., 2020; Saxena et al., 2021; Johnson et al., 2022; Duarte et al., 2023; Yu et al., 2023; Esmaeili et al., 2024; Faria et al., 2025; Lv et al., 2025; Paucar et al., 2025; Ransinangue et al., 2025). However, ML applications based on already existing datasets derived from petrographic samples are absent.

Since petrographic data is widely available for reservoir lithologies globally and can be linked to porosity and permeability datasets, leveraging this resource through machine learning (as a data science application) could reduce drilling costs while maintaining insight into reservoir quality and its controls. Applying these methods to legacy datasets may broaden their use in reservoir geology, especially in the context of the energy transition and increased geothermal or storage applications in fractured and porous rocks with other business cases than classical E&P industry approaches, but is also applicable to mature basins.

Traditional reservoir quality assessments rely on petrophysical routine core analyses, macroscopic and microscopic observations, and well log correlations (Ajdukiewicz and Lander, 2010; Rider and Kennedy, 2011; Worden et al., 2018). These analyses help identifying depositional environments, mineralogical features, and textural properties that influence reservoir quality. Building on proven methods that correlate core data with petrographic analyses, this study uses petrographic datasets and porosity/permeability analyses in two supervised machine learning models (both using Histogram-based Gradient Boosting Regression Trees) to predict porosity and permeability. Rather than algorithm benchmarking, this study aims to highlight the methodological feasibility. With proper calibration, these models could estimate these properties from petrographic samples prepared from e.g., cuttings (e.g., Radwan, 2022; Ölmez et al., 2025) or core pieces with unsuitable dimensions for standard lab analyses of trained lithologies. As cuttings are produced as a by-product of every drilling operation anyways, their petrographic analysis may unlock a greater understanding of reservoir properties in uncored sections, while still understanding variable reservoir quality controls along the well section. Combined with well log data, which is typically available along extended well sections, this approach maximizes the use of data and samples provided during drilling. This would also extend the information gained from uncored well sections, due to limited core retrieval in most cases due to budget constraints. We furthermore evaluate the possibility to utilize data prepared by various petrographers across more than two decades, capturing different petrographic reservoir quality controls from four reservoir lithologies in central Europe, following the initial proof-of-concept that machine learning can be applied to point-counting data (Sadrikhanloo et al., 2026). This will shed light into the influence of operator bias during petrographic analyses and includes the variability in petrographic classes related to different petrographers and lithologies. Furthermore, based on this dataset from 51 wells, we can assess if model performance is comparable if a number of wells are not included in the training and testing data, to assess model robustness and model predictions for single wells. Lastly, we assess if machine learning approaches to these datasets show a better performance than predictions based on a linear regression baseline using only petrophysically or optically determined porosity.

Additionally, SHAP plots (SHapley Additive exPlanations, Lundberg and Lee, 2017) are used to identify which petrographic features influence predictions. When interpreted geologically, these evaluations may reveal previously unknown reservoir quality controls and their interactions. With appropriate calibration data, this method could be applied to reservoir systems worldwide, either to build in-house reference cases for reservoir lithologies in individual basins or combine data from multiple basins to create an overarching model to assess reservoir quality controls and predict key petrophysical properties based on petrographic analyses.

2. Materials and methods

2.1. Geological input data

To test the applicability of machine learning on petrographic and petrophysical reservoir quality data, we compiled a database covering petrographic datasets with associated porosity and permeability data from 51 wells from onshore Germany and offshore The Netherlands. German onshore datasets are derived from published in-house studies (Busch et al., 2019, 2022, 2024, 2025; Monsees et al., 2020), while Dutch offshore datasets were extracted from reports published between 2000 and 2025 available at nlog.nl (Nederlandse Olie-en Gasportaal) (Anderson et al., 2000; Cater, 2001c, b, a; Burfoot et al., 2002a; Burfoot et al., 2002b; Adelmann, 2003; Boels, 2003; Rieke, 2003; van Dijk, 2003; Adelmann, 2004; Boels and Nortier, 2004; Burfoot et al., 2004; Baunack, 2005; Burfoot et al., 2005; John, 2005; Nortier, 2005; Nortier et al., 2005; Nortier and Boels, 2005; John, 2006; John and Baunack, 2006; Morano et al., 2007; Nortier, 2007; RedRock Associates International Limited, 2007; Schaefer et al., 2008; Burfoot et al., 2009; Felder, 2009, 2010a, b; Felder and Pierau, 2010a, b; Mendoza and Felder, 2010a, b; Felder, 2013; Felder and Pierau, 2013; Petrea and Goldberg, 2013; Meier et al., 2014; Petrea and Meier, 2014; Sadlok et al., 2014; Kneen and Petrea, 2015; Felder et al., 2016). The reports from nlog.nl were extracted based on the following criteria: i) The targeted reservoir lithology is siliciclastic. ii) More than one well targets this stratigraphic level. iii) Petrographic and petrophysical data is available for the same samples. For the data compilation, the Well ID from reports was adjusted to match the ID given in the nlog.nl repository.

The studied samples cover Upper Carboniferous fluvio-deltaic sandstones (N = 155), Permian Rotliegendes fluvio-eolian sandstones (N = 295), Lower Triassic Buntsandstein fluvio-eolian to playa margin sandstones (N = 311), and Jurassic marine sandstones (N = 114). The overall dataset comprises 875 samples (850 samples with porosity values, 790 samples with permeability data), covering a porosity range from 0 to 34% and permeability range from 0.001 to >10,000 mD (Fig. 1b). The sandstone classification according to Folk (1980) reveals that samples from all studied wells fall into all categories but with the vast majority with a normalized quartz grain content >50% (Fig. 1a). All utilized data is provided in supplementary materials 1.

The present-day burial depths of the samples range from ~510 to ~5510 m TVD, to assess the model performance in relation to different present-day burial depths. However, as the degree of compaction and cementation recorded in the sandstones is a function of the burial history, and since some samples were relatively uplifted to their paleo maximum burial depths, the present-day burial depth does not correlate to specific reservoir qualities in the studied samples, as e.g., samples with the shallowest present-day burial depths (Well D (Buntsandstein)) have among the lowest average porosity and permeability of the studied samples. In addition, the effect of varying effective stress histories (as recorded by the IGV), thermal exposure and associated fluid-rock interaction (as recorded by contents of e.g., authigenic quartz and illite cements) are recorded in the individual rock microstructure (Fig. 1c–e) assessed during point-counting to prepare the original input data.

To test the robustness of the model we also use samples from four lithological groups from different depositional systems having different provenance areas during the Upper Carboniferous to Jurassic, respectively. Furthermore, the data is created by a variety of petrographers across more than two decades, introducing heterogeneity in the classification of detrital and authigenic phases. However, as the detrital phases also vary as a function of the depositional environment (e.g., ooids in Lower Triassic samples or glauconite in Upper Jurassic samples, Fig. 1d and e) and provenance, the inconsistencies introduced by different petrographers may not be very pronounced in the overall

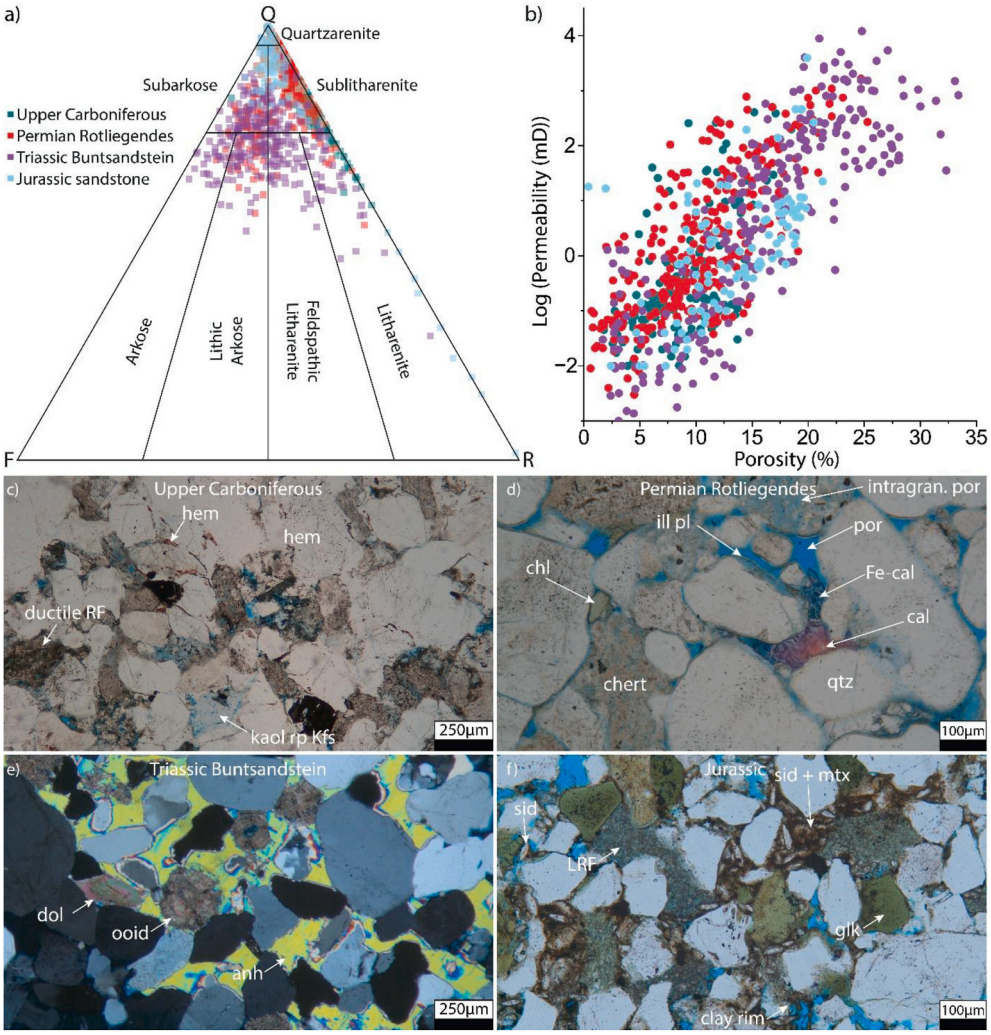

Fig. 1. a) QFR plot of the sample suite color-coded by stratigraphy. b) Porosity-permeability plot of the studied samples, color-coded by stratigraphy. c-e) Exemplary petrographic images showing the differences in detrital and authigenic composition, compaction, and porosity. anh: anhydrite, cal: calcite, chl: chlorite, dol: dolomite, Fe-cal: ferroan calcite, glk: glauconite, hem: hematite, ill: illite, kaol: kaolinite, Kfs: K-feldspar, LRF: limestone rock fragment, mtx: matrix, pl: pore-lining, por: porosity, qtz: quartz, rp: replaces, sid: siderite.

dataset. In addition, the measurement conditions for porosity and permeability (e.g., type of gas/liquid used as permeant or for porosity determination, confining stress, Klinkenberg/Forchheimer-correction applied or not, etc.) are not consistently specified. However, different permeants, confining stresses, and corrections affect porosity and permeability measurements leading to possible deviations when comparing the data from different sources. The data is used as provided in reports, but future applications should account for measurement differences and discuss the influence of this heterogeneity on model predictions. The utilization of a database definitely containing operator/petrographer bias, differing petrophysical measurement protocols, and lithological variety and the discussion of obtained accuracy will be addressed.

Prior to model setup the petrographic data was checked for consistency, and corrected if inconsistent. For example, in some reports the detrital and authigenic mineral contents (excluding the porosity) were summed up to 100% and the optical porosity was given separately. These data were recalculated to add up to 100% including the optically determined porosity. Furthermore, the reports often indicate the presence of minerals in "traces". For simplification and model digestion the occurrence in "traces" has been included as a value of 0.1%. Therefore, the sum of provided point-counting data may exceed 100%. The detrital grain size and sorting can commonly be related to also affect porosity and permeability (Beard and Weyl, 1973). However, since available data for published sample series are heterogeneous (either giving grain size ranges, categorical classifications, or average or median grain sizes, either from core description or petrographic analyses), they have been omitted. Further information on sample material and data can be gained from the original source publications.

The dataset comprises petrographic data (detrital and authigenic phases, optical porosity, IGV), sample depth, and petrophysical data (porosity and permeability). The calculation of IGV is based on Houseknecht (1987), as the sum of intergranular porosity and intergranular cements. High IGV values (up to $>$ 40%) are related to early diagenetic, pre-compaction carbonate/sulphate cementation in both, marine and continental depositional systems, or pervasive early and burial diagenetic silicate cementation.

2.2. Machine learning setup

In total the dataset contains 112 features (see supplementary materials I, indicated by bold box) with porosity and permeability set as the target variables for each of the models, respectively.

For both predictions we used a Histogram-based Gradient Boosting Regression Tree model (HGB) (e.g., Guryanov, 2019; Bentéjac et al., 2020; Shahani et al., 2021; Nhat-Duc and Van-Duc, 2023; Xia et al.,

2024), an ensemble-based algorithm that constructs decision trees during training and outputs the average prediction for regression tasks. HGB accelerates model training by discretizing (binning) input variables (features) to fewer unique values. Furthermore, gradient boosted ensemble methods show robust performance regardless of feature scaling/normalization (Pinheiro et al., 2025), which simplifies the interpretability of predicted values. The process of boosting combines sequentially generated less accurate prediction models to a single more accurate model. HGB was chosen as it natively supports missing values and is generally described as an efficient and fast machine learning algorithm. This manuscript solely presents the outcomes of a single machine learning algorithm to showcase methodological feasibility of machine learning approaches to this type of data, rather than algorithm benchmarking, and outlines its potential use cases. Comparisons of the performance of different algorithms can be found in literature (e.g., Guryanov, 2019; Bentéjac et al., 2020; Shahani et al., 2021; Duarte et al., 2023; Xia et al., 2024).

Prior to model setup, the available data was randomly split into two groups (80% for training and validation, 20% testing). k-fold cross validation (CV) was used for the training and validation data set to assess the robustness of the resulting model. We used 5-fold CV for both models. Hyperparameter tuning was conducted to optimize the learning rate, maximum tree depth, maximum leafs per node, and minimum samples per leaf. For hyperparameter optimization, we first conducted a random search through a broad parameter space, and followed that by an exhaustive grid search around the best-performing set of hyperparameters given by the random search. During optimization, feature selection was not employed, to maintain a more complete picture of feature interactions and to maintain geological interpretability.

Given the large range of permeability values across the dataset, a log-transformation was applied to the target variable (Fig. 2) before training the permeability prediction model. This transformation helped stabilize variance and improved model interpretability, especially in regard to prediction errors. The model performance was assessed using the coefficient of determination (R^2), mean absolute error (MAE), and root mean square error (RMSE), as also suggested by Male and Duncan (2020).

Feature importance was analyzed using SHAP values (SHapley Additive exPlanations, Lundberg and Lee, 2017), providing insights into the effect of specific features on model predictions, as well as their relation with other features. SHAP values are additive, starting from the expected base value of the predicted property (E[f(x)]) if all features were to be unknown (Lundberg and Lee, 2017). The sum of the base value and the SHAP value for each feature gives the predicted value (Lundberg and Lee, 2017). A positive SHAP value of a feature will thus increase the predicted value (positive contribution), while a negative SHAP value decreases the predicted value (negative contribution). The SHAP plots are based on the training data, as this dataset contains more samples and correlations are more clearly visible. For 4 samples (one of each stratigraphic level), we also created SHAP waterfall plots, indicating the specific contribution of the nine most important features on model predictions. The samples were selected using a random number generator and the ID of each sample from 0 to 874. The first randomly selected sample of each stratigraphic level was used.

3. Results and discussion

3.1. Porosity prediction

The predicted porosity values based on petrographic input data show an overall good agreement with petrophysically determined values (Fig. 3). The R^2 of the measured versus predicted porosity for the test data is high at 0.87, the MAE of 1.77 % and RMSE of 2.23% are both low. Furthermore, the metrics are in the same range, as metrics from cross-validation (R^2 = 0.82, MAE = 1.94%, RMSE = 2.58%), implying that the model is not overfitting (Table 1). These metrics imply a robust performance of the porosity prediction based on petrographic data. The errors are acceptable considering the performance in predicting porosity from four different stratigraphic levels and 51 wells, and porosity

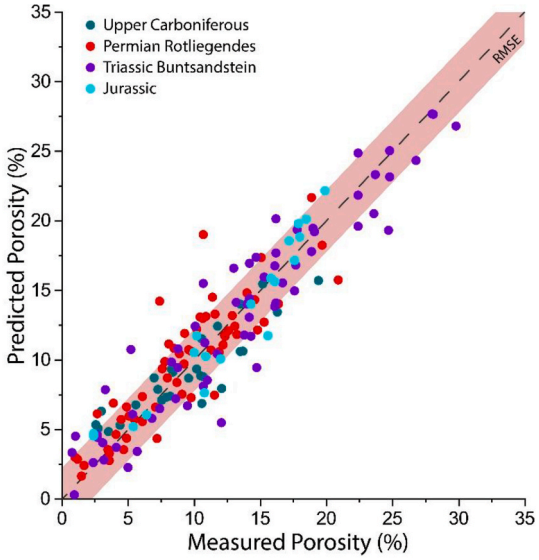

Fig. 3. *Measured versus predicted porosity values for the 170 test samples from all studied wells. The shaded area outlines the RMSE (2.23%) around the 1:1 correlation line.*

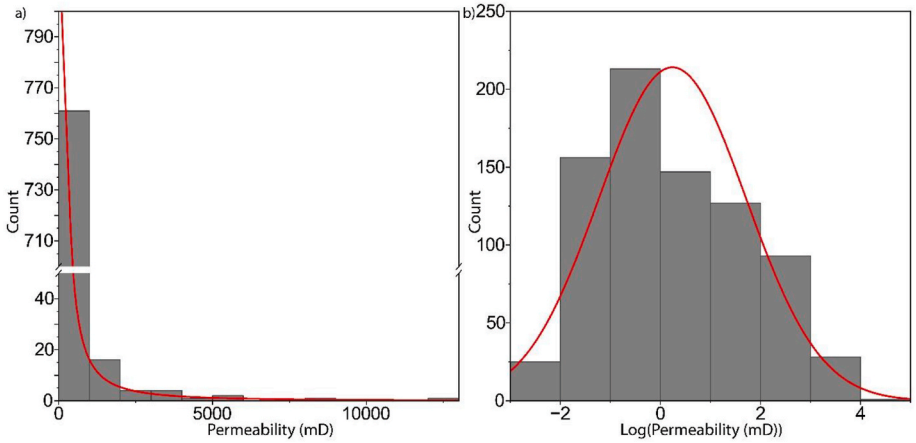

Fig. 2. Histograms of a) the permeability distribution, and b) the log-transformed permeability distribution.

Table 1
Comparison of model metrics of the testing and training/validation (CV) datasets of the porosity and permeability prediction models.

		Porosity model	Permeability model
Test	R^2	0.87	0.82
	MAE	1.77%	0.47
	RMSE	2.23%	0.64
Avg. CV Metrics	R^2	0.82	0.75
	MAE	1.94%	0.54
	RMSE	2.58%	0.72

ranging from 0 to 34%. Furthermore, none of the stratigraphic levels is consistently under- or overpredicted.

3.2. Feature analysis for porosity prediction

SHAP value evaluations allow the assessment which values/contents of individual features positively or negatively affect model predictions. In cases where high feature contents result in high positive SHAP values, we report a positive correlation, whereas low or high feature contents result in high or low SHAP values, we report a negative correlation.

Based on beeswarm plot evaluation (Fig. 4), the most impactful features for porosity prediction are the intergranular porosity (positive correlation), core depth (negative correlation), intergranular dissolution porosity, glauconite content, detrital clay mineral matrix content, polycrystalline quartz grain content, pore-filling kaolinite content (all positively correlated), monocrystalline quartz content (only low contents positively or negatively affect model predictions), and ferroan dolomite contents (negative correlation).

Further insight into the model predictions can be gained from SHAP dependence plots (Fig. 5). The SHAP dependence plots illustrate the relationship between individual features (plotted along the x-axis and used for the color-code) and their impact on porosity predictions. These interactions help reveal how two features jointly influence porosity, capturing complex dependencies beyond simple correlations and, when linked to geological reasoning, can aid in understanding reservoir quality controls related to detrital components or authigenic minerals and processes.

Unsurprisingly, intergranular porosity from point-counting shows a positive, non-linear relationship with plug porosity measurements (Fig. 5a). Positive SHAP values indicate a positive influence on the target property. Thus, higher point-counted intergranular porosity corresponds to higher predicted plug porosity. The non-linearity can be related to the fact that optical porosity from point-counting analyses often underestimates microporosity (e.g., within clay minerals) (Hurst and Nadeau, 1995). Intergranular porosity also interacts with secondary intragranular (dissolution) porosity, where samples with higher secondary intragranular porosity contents receive greater positive contributions to predicted porosity for a given intergranular porosity content. Similarly, secondary intragranular porosity positively affects model predictions (Fig. 5b). Higher contents of secondary intragranular porosity (mostly <10%) show positive SHAP values implying a positive influence on predicted porosity. The feature interaction with intergranular porosity shows that samples with higher intergranular porosity have a lower contribution to predicted porosity than samples with similar secondary intragranular but lower intergranular porosity.

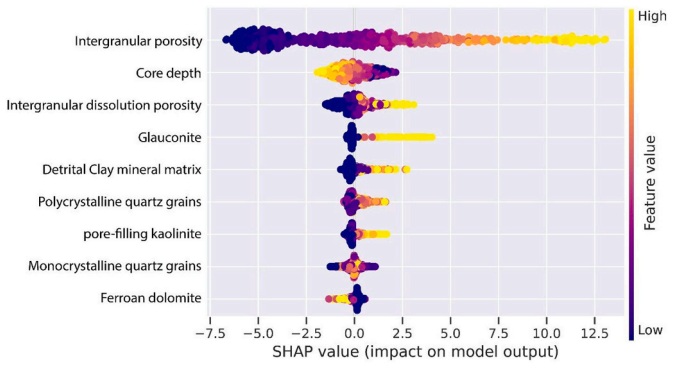

Fig. 4. Beeswarm plot highlighting the contributions of individual feature values on the predicted porosity.

Core depth also influences porosity, with deeper samples showing negative SHAP values, indicating a negative effect on predicted porosities (Fig. 5c). This likely reflects stronger compaction and cementation in more deeply buried intervals (e.g., Paxton et al., 2002). When considering the interaction with intergranular porosity, samples deeper than ~2500 m with higher intergranular porosity receive a more negative depth-related contribution than samples with lower intergranular porosity.

Although not among the nine most influential features, pore-filling and pore-lining illite still show notable correlations with predicted porosity (Fig. 5d and e). Small amounts of pore-filling illite (<4%) can have either a positive or negative effect, but higher contents (>4%) generally contribute positively, likely because pore-filling illite is often associated with feldspar dissolution and may act as a grain-coating phase that inhibits quartz cementation and preserves porosity (e.g., Busch et al., 2024). The influence of pore-filling illite also depends on intergranular porosity, as samples with higher intergranular porosity consistently receive lower, and sometimes negative, contributions compared with samples having lower intergranular porosity.

Pore-lining illite contents below 3% positively affect porosity predictions, while contents above 3% mostly negatively affect model predictions (Fig. 5e). While pore-lining illite can be an effective grain coating mineral phase (e.g., Storvoll et al., 2002) reducing the content of syntaxial quartz overgrowth cements, which in turn may results in higher preserved porosity (Fig. 6b and c), if present at grain-to-grain contacts, it also enhances the effect of chemical compaction (i.e., pressure dissolution) (Kristiansen et al., 2011; Monsees et al., 2020), reducing porosity. Feature interactions show that samples with higher monocrystalline quartz grain content receive a stronger negative contribution to the prediction than those with lower monocrystalline quartz grain content at the same pore-lining illite contents.

Detrital clay mineral matrix contents generally positively affect model predictions (Fig. 5f) mostly related to the elevated microporosity contents within clay mineral matrix, which cannot be accurately assessed using transmitted light microscope analysis (Hurst and Nadeau, 1995). The feature interaction shows that samples with higher intergranular porosity contain less clay mineral matrix, and the clay mineral matrix contributes most strongly to predicted porosity in samples with high clay mineral matrix contents and low intergranular porosity.

Pore-filling kaolinite also positively affects model predictions (Fig. 5h). This may be attributed to microporosity in kaolinite and to enhanced secondary intragranular porosity, often associated with the presence of kaolinite and genetically related to the dissolution of feldspar grains and precipitation of kaolinite (Lanson et al., 2002). Feature interaction shows that this influence depends on intergranular porosity. At low kaolinite contents (<5%), samples with higher intergranular porosity receive lower contributions than those with similar kaolinite contents but lower intergranular porosity. At higher kaolinite contents, this relationship reverses, with samples containing both abundant pore-filling kaolinite and high intergranular porosity receiving the strongest positive contributions.

Pore-filling ferroan dolomite contents generally negatively affect model predictions (Fig. 5g). Machine-learning results also capture stratigraphy-specific controls. Only Jurassic samples contain glauconite (Fig. 5i), so only these show positive SHAP contributions, whereas samples without glauconite show zero or slightly negative contributions. Feature interactions also reveal, that samples containing the same amount of ferroan dolomite receive a more negative contribution with

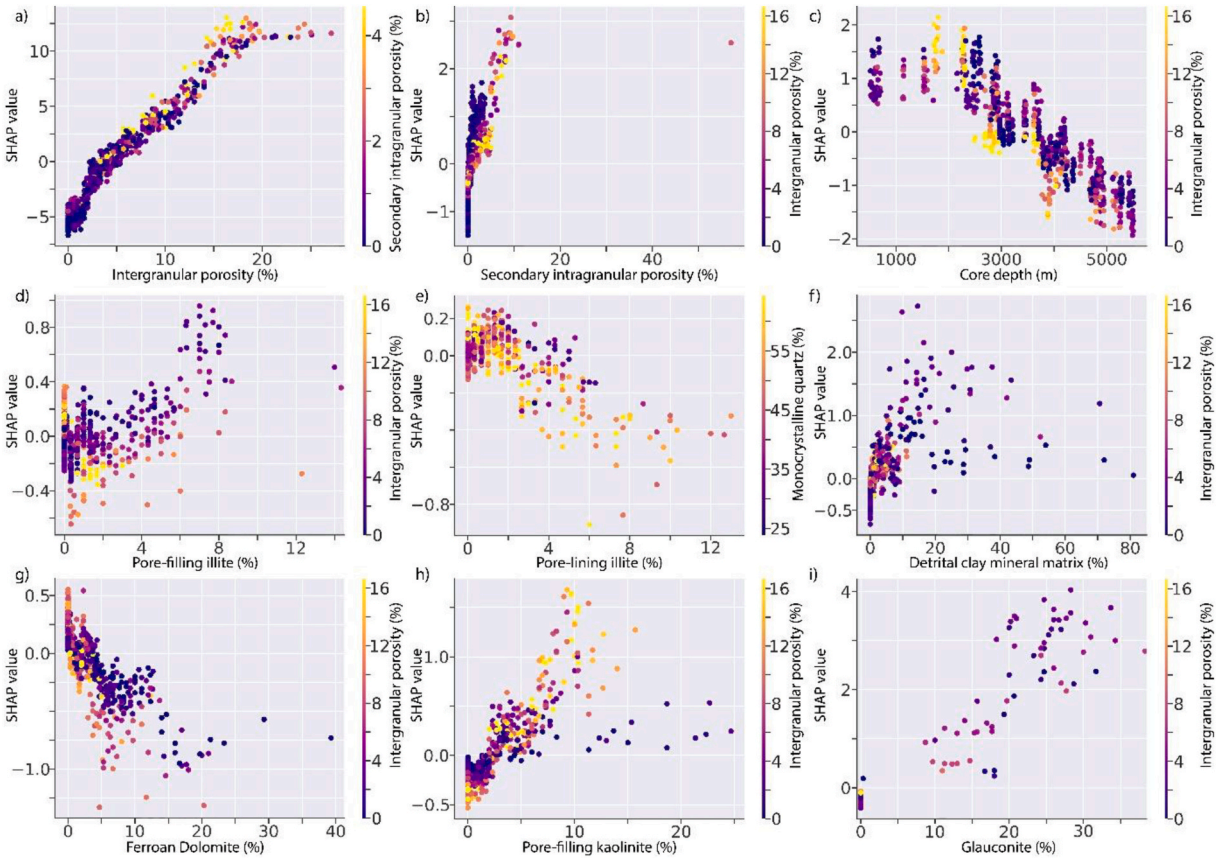

Fig. 5. SHAP dependence plots for a) Intergranular porosity, b) secondary intragranular porosity, c) core depth, d) pore-filling illite, e) pore-lining illite, f) detrital clay mineral matrix, g) ferroan dolomite, h) pore-filling kaolinite, i) glauconite.

increasing intergranular porosity, unless ferroan dolomite is absent. Similarly, the contribution of high glauconite contents to porosity predictions is highest in samples with low intergranular porosity, likely largely related to the microporosity in glauconite pellets (Thomas et al., 2003).

While microporosity cannot be accurately assessed in transmitted light microscopy (Hurst and Nadeau, 1995), the presence of microporous mineral phases (e.g., detrital clay mineral matrix, kaolinite, glauconite, and kaolinite) are among the nine most influential features on porosity prediction (Fig. 4). Therefore, although microporosity was not explicitly included as a point-counting category, its influence on model predictions is implicit, as the model assigns high feature importance to microporous mineral phases.

Based on the expected base value of the predicted porosity (E[f(x)] = 11.73), SHAP waterfall plots correlate the feature properties of specific samples to their contribution to the predicted porosity (Fig. 7).

The porosity prediction for the Upper Carboniferous sample is negatively affected by the low pseudomatrix content, high indeterminate rock fragment content, low monocrystalline quartz grain content, low detrital clay mineral matrix content, low ferroan dolomite content, and low quartz cement content. Further negative contributions are the great core depth and the sum of 103 other features. The prediction is positively affected by the high intercrystalline microporosity and high intergranular porosity (Fig. 7a).

The prediction for the Permian Rotliegendes sample is negatively affected by the low intergranular porosity, high K-feldspar grain content, low IGV, low metamorphic rock fragment content, low detrital clay mineral matrix content, low pore-filling kaolinite content, and low claystone rock fragment content. The remaining 103 features also negatively contribute to the predicted porosity. Small positive contributions are from the low secondary intragranular porosity and low non-ferroan dolomite content, resulting in lower predicted porosities than for the Upper Carboniferous sample (Fig. 7b).

The porosity prediction for the Triassic Buntsandstein sample is negatively affected by the core depth, low pore-filling kaolinite content, low detrital clay mineral matrix content, low IGV, and low feldspar cement content. The remaining 103 features also negatively affect model predictions. However, the high replacive clay mineral content, high intergranular dissolution porosity, moderate polycrystalline quartz grain content and moderate intergranular porosity positively affect model predictions, resulting in higher predicted porosity than in the previous two samples (Fig. 7c).

The porosity prediction of the Jurassic sample is only negatively affected by the presence of anhydrite clasts, whereas the high secondary intragranular porosity, high halite cement content, detrital clay mineral rim content, high detrital clay mineral matrix content, and high glauconite content, as well as low K-feldspar grain content, low heavy mineral content, low IGV, and the sum of the remaining 103 features all positively affect the predicted porosity (Fig. 7d).

3.3. Permeability prediction

Permeability values in the studied sample suites exhibit a right-skewed, approximately log-normal distribution (Fig. 2a and b), spanning nearly eight orders of magnitude. Log-transformed permeability predictions using the HGB model show a very good agreement with petrophysically derived values, with a high R^2 of 0.82, a MAE of 0.47, and RMSE of 0.64 (Fig. 8). Furthermore, the metrics are in the same range, as metrics from cross-validation (R^2 = 0.75, MAE = 0.54, RMSE = 0.72), implying that the model is not overfitting (Table 1). Given the approximately log-normal distribution of the data, these values indicate that predictions generally fall within 0.64 orders of magnitude of the

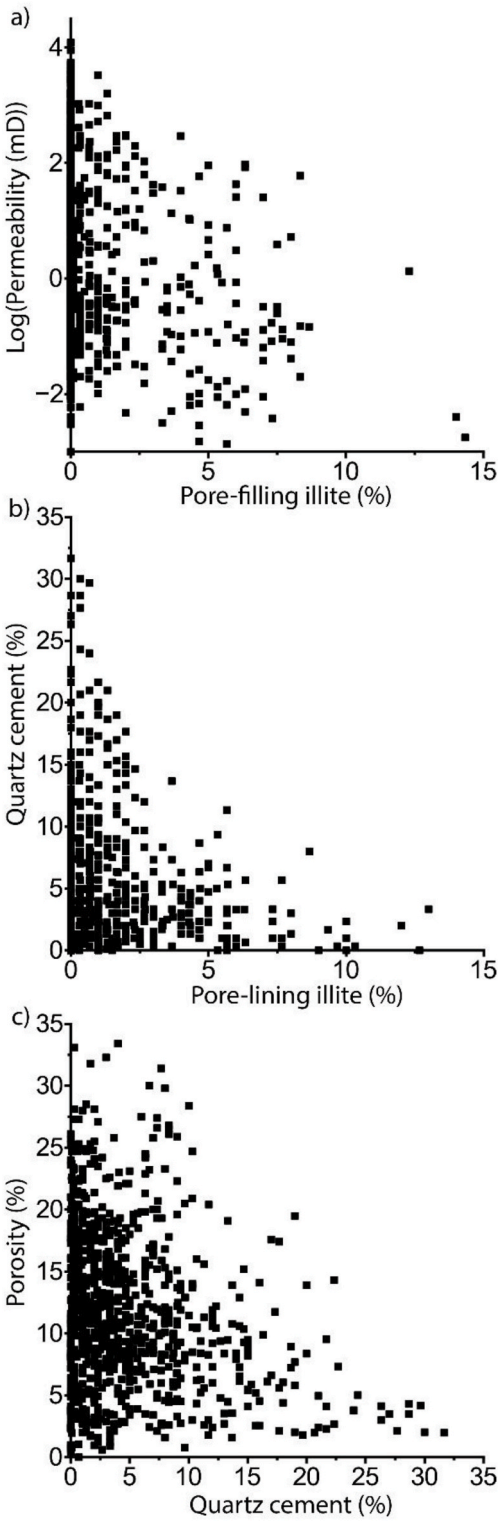

Fig. 6. Correlations of petrographic and petrophysical data. a) Pore-filling illite content vs. permeability. b) Pore-lining illite vs. quartz cement. c) Quartz cement vs. porosity. Quartz cement contents above 20% are mostly related to high thermal exposure and low grain coating coverages (e.g., Fig. 7e in Busch et al., 2024).

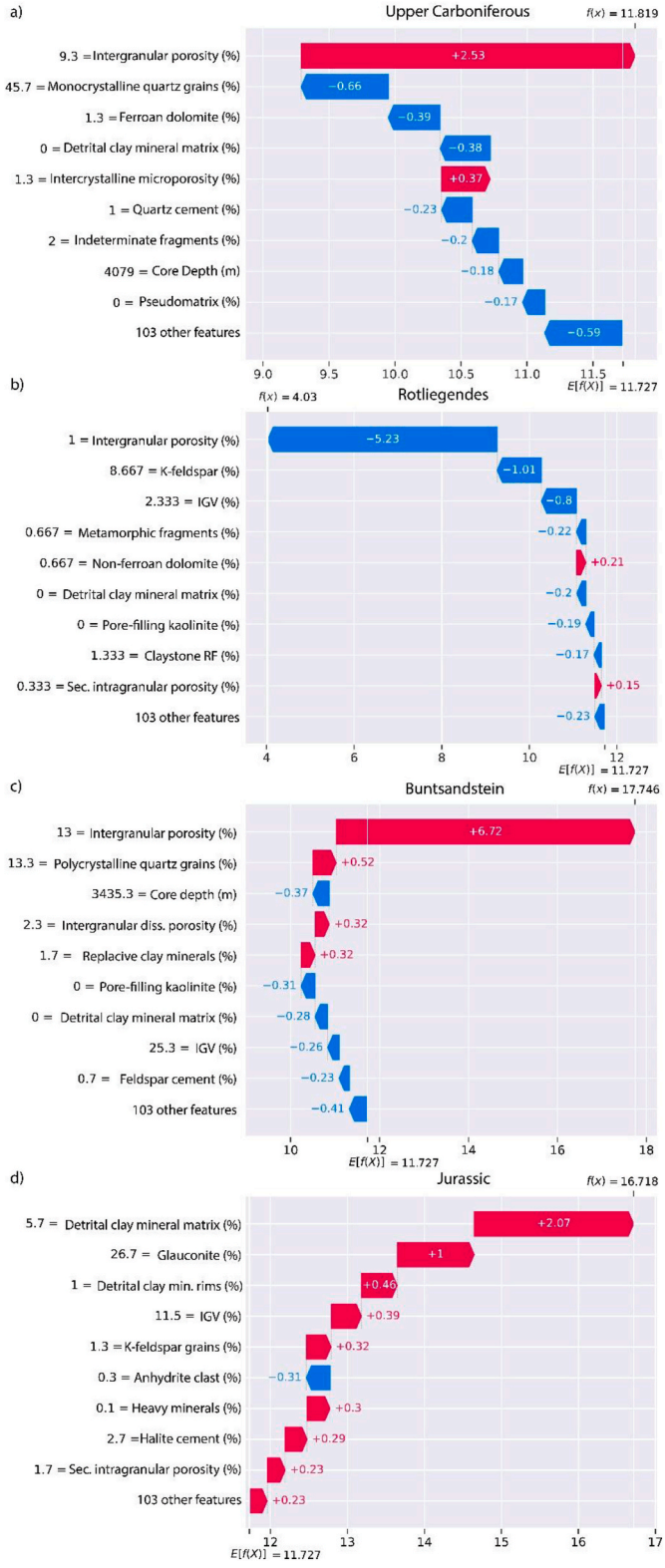

Fig. 7. SHAP waterfall plot for porosity prediction for a) an Upper Carboniferous sample (ID = 29), b) a Permian Rotliegendes sample (ID = 778), c) a Triassic Buntsandstein sample (ID = 79), and d) a Jurassic sample (ID = 445).

measured permeability values. Considering the data's broad dynamic range, these errors are acceptable, supporting the conclusion that permeability can be reasonably predicted within one order of magnitude, an appropriate scale for practical reservoir characterization. Furthermore, none of the stratigraphic levels is consistently under- or overpredicted, implying a robust performance, regardless of rock composition.

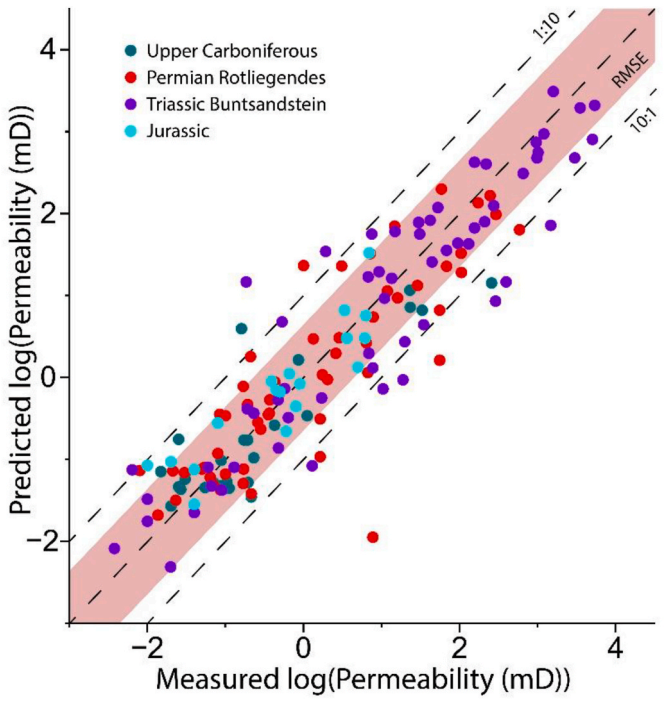

Fig. 8. Measured versus predicted permeability values for the 158 test samples from the studied wells. The shaded area outlines the RMSE (0.64) around the 1:1 correlation line.

3.4. *Feature analysis for permeability prediction*

Based on beeswarm plot evaluation (Fig. 9), the most impactful features for permeability prediction are the intergranular porosity, polycrystalline quartz grains (both positively correlated), core depth (only low contents strongly negatively affect model predictions), pore-filling illite, ferroan dolomite, pore-lining illite, indeterminate fragments, IGV (all negatively correlated), and intergranular dissolution porosity (positive correlation) contents.

The intergranular porosity from point-counting analyses shows a positive, non-linear relationship with plug permeability predictions (Fig. 10a). Intergranular porosity above ~5% contributes positively to predicted permeability, whereas values below 5% contribute negatively. Feature interactions (color-code) show that samples with intergranular porosity >5% receive a lower contribution at higher pore-filling clay mineral contents. The opposite is the case for samples containing intergranular porosities <5%.

Similarly, secondary intergranular porosity (i.e., dissolution porosity after intergranular cements) positively affects model predictions

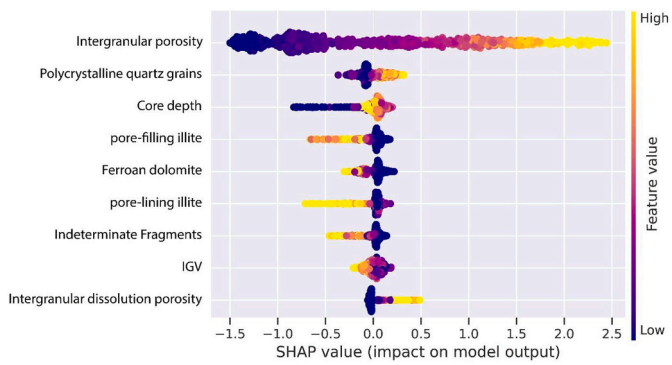

Fig. 9. Beeswarm plot highlighting the contributions of individual feature values on the predicted permeability.

(Fig. 10b). However, the contribution toward the permeability prediction is also affected by the intergranular porosity of each sample, with samples having a low intergranular porosity, receiving a higher contribution than samples with high intergranular porosity.

An increase in IGV is generally associated to a more negative contribution to the permeability prediction (Fig. 10c), largely related to higher intergranular cement contents (Fig. 11b). Assessing the feature interaction, the contribution of the IGV is also related to the intergranular porosity, with a change of the relationship around SHAP values of 0. Both, positive and negative contributions are greater for samples with higher intergranular porosities.

Higher ferroan and non-ferroan dolomite contents negatively affect permeability predictions (Fig. 10h and i), whereas low amounts or absence of these cements have a positive influence. For ferroan dolomite, the contribution also depends on core depth. More shallow samples receive a stronger negative effect at ~5% ferroan dolomite, likely reflecting the framework-stabilizing role of pore-filling cements at greater depths. Non-ferroan dolomite shows a weak interaction with plutonic rock fragments, where samples with higher plutonic fragment contents receive lower contributions to predicted permeability than those with fewer fragments at the same dolomite content.

Shallower burial depths generally negatively affect permeability predictions (Fig. 10d). This is largely related to the inclusion of e.g., well samples from inverted lithologies (Well D Buntsandstein, Busch et al. (2025)). When considering only samples between ~2500 and 5500 m depth, deeper burial more strongly reduces predicted permeability, reflecting higher thermal exposure and greater cement volumes (Fig. 11a). However, at depths >~2500 m, samples with higher intergranular porosity receive smaller, or even negative, contributions to predicted permeability.

Pore-filling and pore-lining illite generally negatively affect model predictions (Fig. 10e and f). Similar to porosity predictions, permeability predictions are sensitive to pore-filling illite contents, as they reduce the effective pore throat radii, negatively affecting fluid flow (Fig. 6a). This is supported by Neasham (1977), who found lower permeabilities in sandstones containing radial illite textures. Pore-filling illite also interacts with intergranular porosity. At contents >~3%, samples with higher intergranular porosity receive more negative contributions than those with lower intergranular porosity.

Pore-lining illite contents <~4% still record a positive influence on permeability, likely related to the inhibition of syntaxial cement overgrowths, but higher contents negatively influence permeability predictions, in part related to the enhanced chemical compaction along illite-coated grain contacts (Busch et al., 2024). The feature interaction again highlights an influence of the intergranular porosity. Both, positive and negative contributions are smaller for samples with higher intergranular porosities.

Undifferentiated pore-filling clay minerals similarly negatively influence model predictions (Fig. 10g), as they also reduce the hydraulic pore throat radii. However, the feature interaction plot indicates that the effect is more pronounced in samples having higher intergranular porosity.

Based on the expected base value of the predicted permeability (E[f(x)] = 0.27 (log(Permeability (mD))), SHAP waterfall plots correlate the feature properties of specific samples to their contribution to the predicted permeability. The permeability prediction for the Upper Carboniferous sample is negatively affected by the high monocrystalline quartz grain content. The prediction is positively affected by the intergranular porosity, oversized porosity, low polycrystalline quartz grain content, low non-ferroan and ferroan dolomite cement content, and low pore-filling illite content, as well as the low IGV, core depth, and the sum of the remaining 103 features, resulting in a high predicted permeability (100s of mD) (Fig. 12a).

The prediction for the Permian Rotliegendes sample is negatively affected by the low intergranular porosity, shallow core depth, high pore-lining and pore-filling illite content, high chert content, low

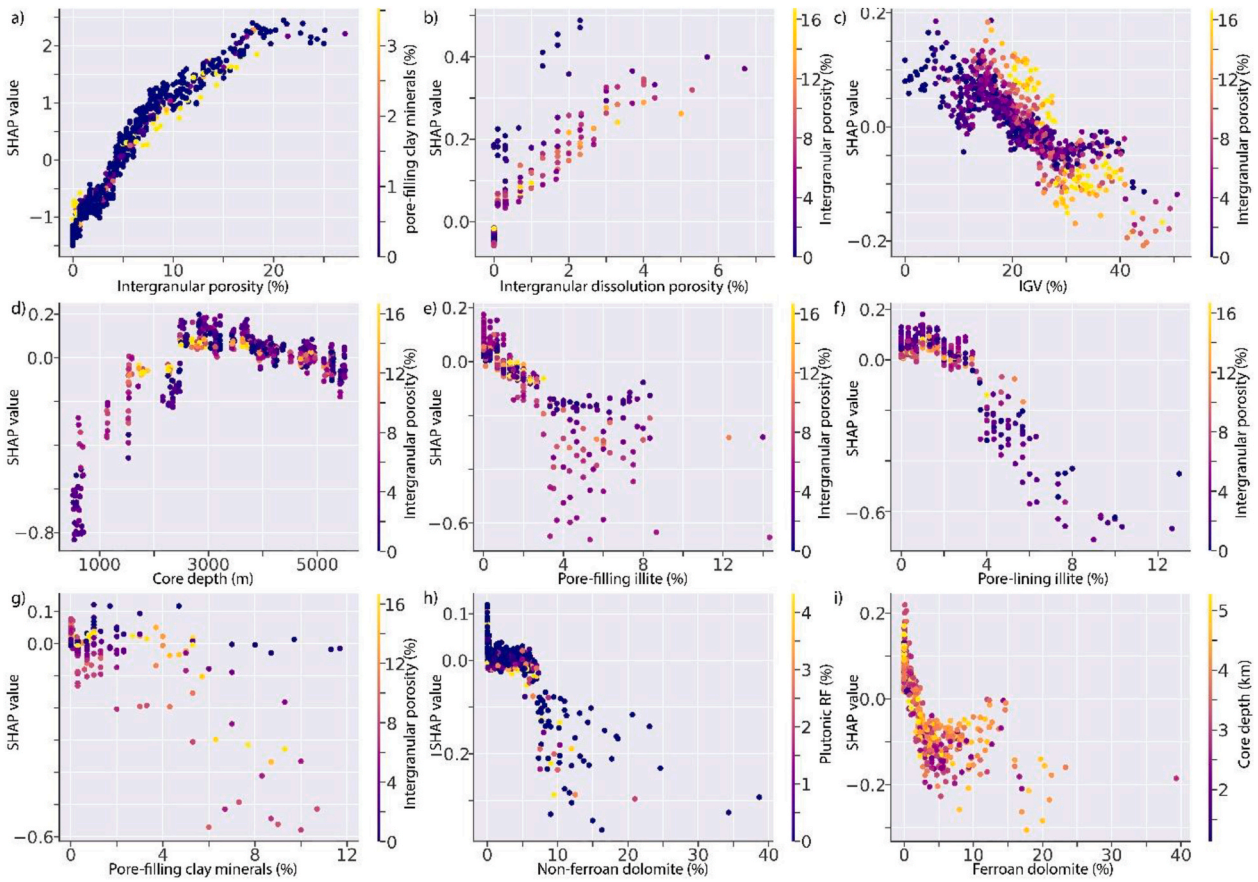

Fig. 10. SHAP dependence plots for a) Intergranular porosity, b) Secondary intergranular porosity, c) IGV, d) core depth, e) pore-filling illite, f) pore-lining illite, g) pore-filling clay minerals, h) non-ferroan dolomite, and i) ferroan dolomite.

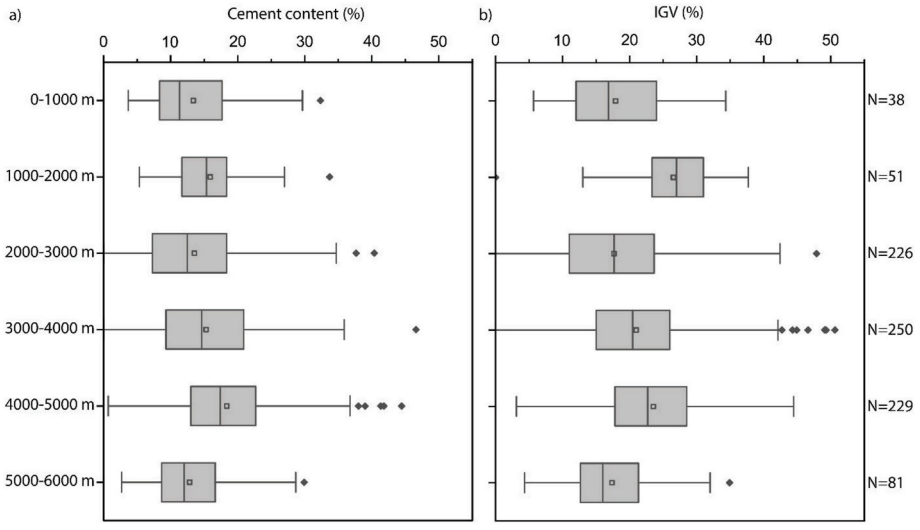

Fig. 11. a) Cement content and b) IGV versus depth. With increasing depth greater than 2000 m cement volume and IGV both slightly increase.

polycrystalline quartz grain content, low biotite content, and low intergranular dissolution porosity. The remaining 103 features also negatively contribute to the predicted permeability. Small positive contributions are only from the low ferroan dolomite content, resulting in lower predicted permeability (0.001s of mD) than for the Upper Carboniferous sample (Fig. 12b).

The permeability prediction for the Triassic Buntsandstein sample is only negatively affected by the high plagioclase content. The remaining 103 features, low barite cement content, low pore-filling kaolinite and illite contents, low ferroan dolomite content, high polycrystalline quartz grain content, intergranular dissolution porosity, and high intergranular porosity, as well as the moderate core depth all positively affect the predicted permeability (100s of mD) (Fig. 12c).

The permeability prediction of the Jurassic sample is negatively affected by the high pore-filling clay mineral content, low polycrystalline quartz grain content, and high siderite cement content, while

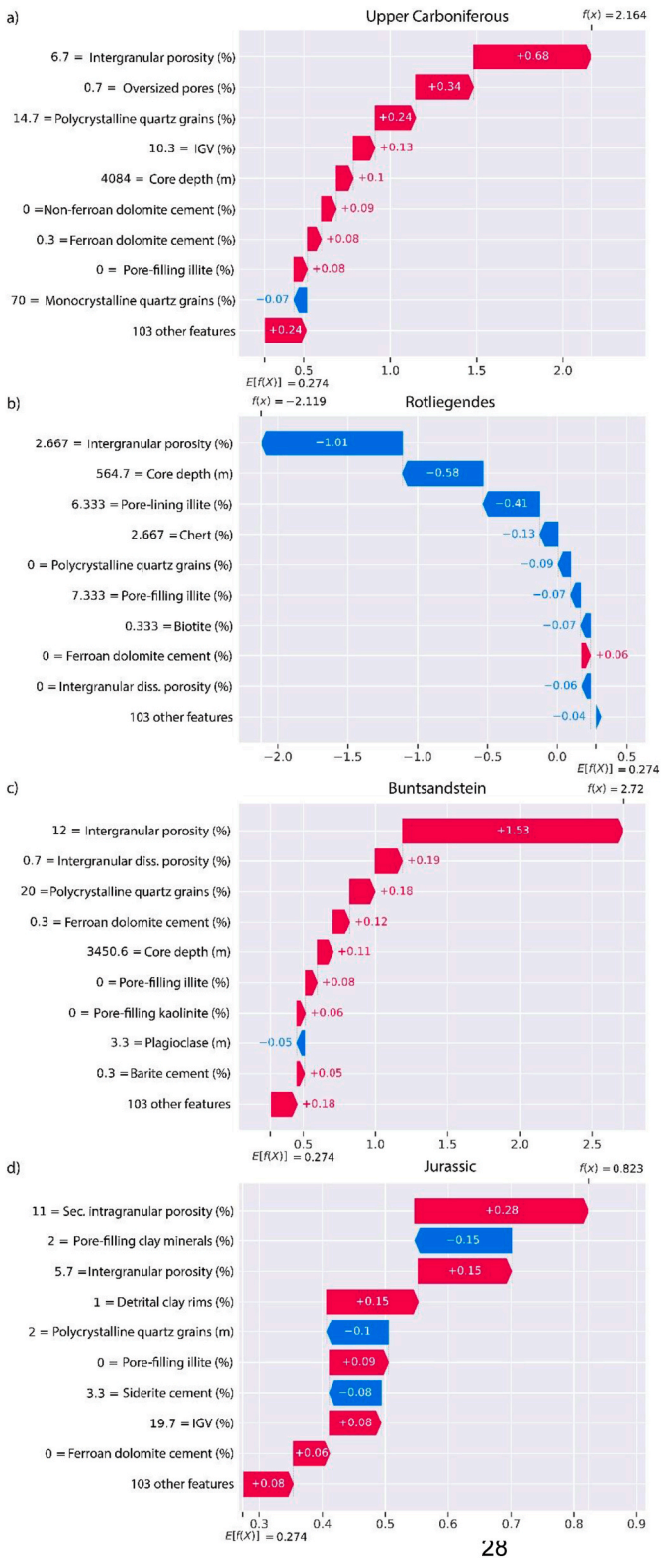

Fig. 12. SHAP waterfall plot for permeability prediction for a) an Upper Carboniferous sample (ID = 29), b) a Permian Rotliegendes sample (ID = 778), c) a Triassic Buntsandstein sample (ID = 79), and d) a Jurassic sample (ID = 445).

the high secondary intragranular porosity, moderate intergranular porosity, detrital clay rim content, low pore-filling illite content, low ferroan dolomite cement content, moderate IGV, and the sum of the remaining 103 features all positively affect the predicted permeability (1s of mD) (Fig. 12d).

3.5. Comparison with linear regression baseline and previous datasets

As the intergranular porosity from point-counting is the main feature influencing porosity and permeability predictions, and porosity and permeability show a general positive correlation, we furthermore assess the performance of linear regression analysis in providing a calculation for porosity and permeability (Table 2).

The linear regression of optically determined porosity (intergranular, secondary, and fracture porosity from point-counting) and petrophysically determined porosity shows an R^2 of 0.65. Calculated porosity from the linear regression equation shows a MAE of 3.92% and a RMSE of 4.33%.

The linear regression of optically determined porosity (intergranular, secondary, and fracture porosity from point-counting) and petrophysically determined log-transformed permeability shows an R^2 of 0.58. Calculated permeability from the linear regression equation shows a MAE of 0.56 and a RMSE of 0.95.

The linear regression of petrophysically determined porosity and petrophysically determined log-transformed permeability shows an R^2 of 0.59. Calculated permeability from the linear regression equation shows a MAE of 0.66 and a RMSE of 0.95.

The used metrics (R^2, MAE, RMSE) for the machine learning-based approaches are all better than the results from linear regression analyses based on a single feature (Table 2). This highlights the ability of machine learning approaches to derive more meaningful porosity and permeability predictions based on petrographic input data, including detrital and authigenic phases in addition to point-counted porosity types.

Comparison to results of the proof-of-concept study (Sadrikhanloo et al., 2026) reveals that although as the mineralogical variety of samples and the number of petrographers was increased, the predictive performance is only slightly reduced (Table 2). However, accuracy is still within one order of magnitude, delivering reasonable predictions. The likeliest reason for this deviation may be the higher dynamic range of the predictors, the non-unified petrographic input characteristics, and non-unified petrophysical measurement protocols.

3.6. Multiple unseen well prediction

To assess the robustness of the model, the complete database was split into three subsets containing wells of each stratigraphic section (N = 243, 310, and 237 samples). The remaining samples of each subset were used as training-validation data to set up individual models using the same hyperparameter range as the models presented above. The wells are sorted by stratigraphy and assigned to one of the subsets from top to bottom. This sorting induces some imbalance in the number of samples per subset, but maintains that samples from all stratigraphic levels are included in each subset. We can thereby test if the model performance is comparable, if subsets of well samples are removed from the training-validation set, and if error metrics for predictions for unseen well samples for each model remain comparable.

For both, the porosity and permeability model, the error metrics for all three subsets remain comparable with each other (Table 3), regardless if the mean cross-validation, testing, or prediction metrics are assessed. In the porosity model, CV and test metrics are very comparable between the subsets, only for the prediction subsets differences can be

Table 2
Comparison of machine learning (HGB, RF, SVR) and linear regression (LR) errors for porosity and permeability prediction based on petrophysically determined porosity (porosity) and optically determined porosity from point-counting (opt. porosity). RF and SVR: The best-performing Random Forest and Support Vector Machine regression models from Sadrikhanloo et al. (2026).

	Porosity			Permeability			
	HGB	RF	LR (opt. porosity)	HGB	SVR	LR (porosity)	LR (opt. porosity)
R^2	0.87	0.92	0.65	0.82	0.83	0.58	0.59
MAE	1.77%	1.25%	3.92%	0.47	0.21	0.66	0.58
RMSE	2.23%	1.56%	4.33%	0.64	0.24	0.95	0.95

Table 3
Comparison of performance of the machine learning models with unseen wells. Both, the porosity and permeability model show comparable metrics for CV and testing datasets for each subset (Subs.), but show slightly higher error metrics for the prediction (Pred.) of unseen samples. StDev: standard deviation.

Porosity Model											
Subs.	N (CV)	N (Pred.)	CV			Test metrics			Prediction		
			R^2	MAE (%)	RMSE (%)	R^2	MAE (%)	RMSE (%)	R^2	MAE (%)	RMSE (%)
1	578	250	0.84	1.99	2.66	0.84	2.20	2.96	0.49	2.87	3.60
2	558	316	0.81	2.01	2.58	0.86	1.91	2.45	0.76	2.68	3.41
3	614	250	0.83	1.98	2.60	0.82	1.96	2.63	0.80	2.33	3.06
		Average	0.83	1.99	2.61	0.84	2.02	2.68	0.68	2.63	3.36
		StDev	0.02	0.02	0.04	0.02	0.15	0.26	0.17	0.28	0.27
Permeability Model											
Subs.	N (CV)	N (Pred.)	CV			Test metrics			Prediction		
			R^2	MAE	RMSE	R^2	MAE	RMSE	R^2	MAE	RMSE
1	547	243	0.77	0.55	0.72	0.81	0.47	0.60	0.65	0.62	0.81
2	480	310	0.70	0.59	0.75	0.78	0.53	0.66	0.64	0.75	0.95
3	553	237	0.74	0.56	0.76	0.82	0.47	0.62	0.63	0.66	0.84
		Average	0.74	0.56	0.74	0.80	0.49	0.63	0.64	0.68	0.87
		StDev	0.04	0.02	0.02	0.02	0.03	0.03	0.01	0.07	0.08

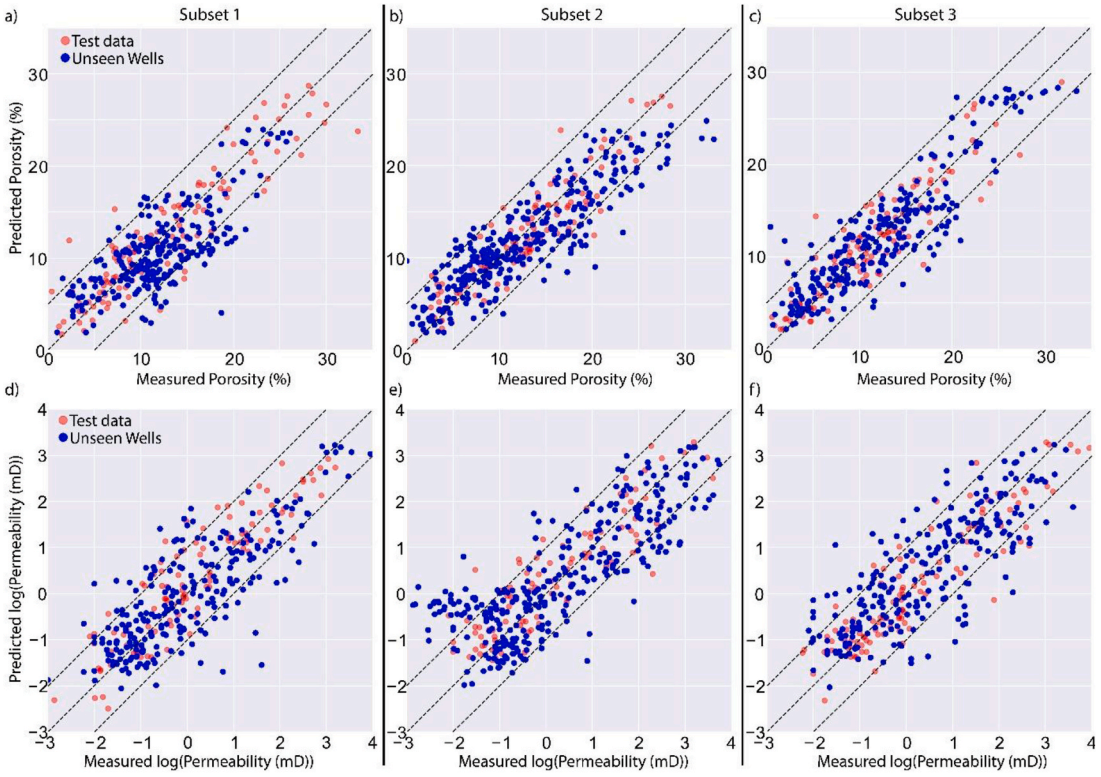

Fig. 13. Correlation of measured and predicted porosity (a-c) and measured and predicted permeability (d-f) for each of the subsets.

observed especially for the R^2 of subset 1. However, the other metrics (MAE and RMSE) for the predictions of this subset are still comparable to the metrics of the other two subsets. This is also supported by visual analysis of the predicted porosity with measured porosity (Fig. 13a–c), where the large majority of predictions fall well within 5 % of the measured value for the unseen wells and samples from the test split of

the training data. The much poorer R^2 value is likely related to the smaller range of porosities in the unseen well samples and large number of samples in the 10-15% porosity range.

While the metrics for the prediction of permeability of samples from unseen wells are slightly lower than the CV and test metrics, they consistently show similar predictive performance with very low standard deviation. We therefore interpret that the model is generally robustly predicting porosity and permeability well within 5% or within an order of magnitude of unseen well samples, regardless of which wells are used for model training.

3.7. Single unseen well prediction

A randomly chosen well (L08-16-S1, Rotliegendes) was extracted from the dataset to assess single unseen well prediction performance. After extraction a model was trained-validated on the remaining well samples in the same hyperparameter space as the initial model. The porosity model metrics for CV and test datasets are very comparable (Table 4). Only the R^2 value of the prediction for the 18 unseen samples is much lower, while the error metrics (MAE and RMSE) are comparable to the metrics of the test dataset. The permeability model metrics for CV and test datasets are again comparable, and the results for the prediction show slightly higher error metrics (MAE and RMSE). However, they are only slightly higher than in the unseen multi-well splits and mostly fall within one order of magnitude (Fig. 14 b). Similarly, porosity predictions are well within 5% of the measured value (Fig. 14 a). We therefore interpret, that for the purpose of practical reservoir characterization, the presented model and general approach can be used to assess porosity and permeability within reasonable errors (5% and one order of magnitude, respectively).

3.8. General discussion

The presented approach successfully showcases the ability of machine learning approaches to derive meaningful porosity and permeability predictions regardless of present-day depths or stratigraphy. As effects of diagenesis and compaction are recorded by the specific petrographic samples (i.e., authigenic mineral content, IGV, and the types and amounts of optically determined porosity) their contents can be related to differences in porosity and permeability.

The robustness of the models is supported by the low errors and their ability to assess porosity and permeability for 875 samples from 51 wells across Germany and the Netherlands covering four stratigraphic sections, characterized by different sediment provenances and depositional environments. Furthermore, the comparable metrics of testing and 5-fold cross-validation data splits (Table 1) imply model robustness.

Porosity and permeability predictions based on this model do not appear to be affected by these differences in depositional environments and provenance, as the specific detrital and authigenic components from point-counting analyses are considered. Even the local abundance of certain grain types (e.g., glauconite in Jurassic wells) does not pose a problem, as the absence of these minerals and grains in other samples does not strongly affect porosity or permeability predictions, based on SHAP plot evaluation (Fig. 5i). Furthermore, porosity and permeability are not systematically over- or underpredicted based on the different stratigraphic sections (Figs. 3 and 8).

Additionally, the data provided by different petrographers across 25 years and formation specific presence of certain grain types and minerals highlights: As long as the influence of a certain mineral and its specific quantity is captured in the training data, the model can still predict meaningful value ranges. This suggests that variable data availability can be handled by data science applications, such as machine learning. The well-wise splits and single well predictive metrics also highlight, that once the model captures the relevant influence on reservoir quality and the used point-counting categories are included in the training dataset, a prediction should yield reasonable results. Therefore, previously perceived challenges including operator bias in petrographic analyses, as utilized datasets span multiple decades and providers and contain a variety of classes, do only slightly influence model performance. This is supported by the similar coefficient of determination (R^2) between a curated dataset (Sadrikhanloo et al., 2026) and this combined dataset (Table 2). The generally slightly larger error metrics (MAE, RMSE) of the combined dataset when compared to the error metrics of the curated dataset is likely due to the overall larger dynamic range of data. This was also observed in the curated dataset, where error metrics were larger for sample series containing a larger range of data (Sadrikhanloo et al., 2026). Another possible reason for a broader dynamic range of the predictors are the measurement conditions of petrophysical analyses. As they are also not consistently specified in all reports, and measurements differ as a function of e.g., permeant and confining stresses, the ranges of reported values could be narrower than presented here. In case of porosity analyses, reported values for the same samples, differ based on the utilized method, often relating to different sizes of molecules used to penetrate the pore space (e.g., Busch et al., 2017a). As helium has a smaller size than e.g., water, mercury, nitrogen, or organic fluids, it may penetrate narrower pore throats and ultimately result in higher reported porosities for the same sample. This possible deviation adds noise to the input data, reducing the apparent model performance, and could mean that results may be conservative, as using helium for all measurements would increase the petrophysically determined porosities. In case of permeability analyses, the used permeant will also affect the measured apparent permeabilities, a circumstance normally corrected for by applying a Klinkenberg-correction where Darcy conditions are met (e.g., Orlander et al., 2021). Apparent permeabilities are higher than Klinkenberg-corrected permeabilities (Klinkenberg, 1941; Rieckmann, 1970). In case of differences in the applied confining stress to avoid sample bypass during permeability measurements or to simulate permeability under reservoir confining stresses, higher effective confining stresses generally reduce measured permeabilities (e.g., David et al., 1994). Therefore, the diverse and sometimes unspecified permeability measurement methods of the compiled database add noise, by both including possibly higher and

Table 4
Single unseen well prediction performance of the machine learning models. Both, the porosity and permeability model show comparable metrics for CV and testing datasets, but show slightly higher error metrics for the prediction (Pred.) of unseen samples.

Porosity model										
N (CV)	N (Pred.)	CV			Test			Prediction		
		R^2	MAE (%)	RMSE (%)	R^2	MAE (%)	RMSE (%)	R^2	MAE (%)	RMSE (%)
832	18	0.84	1.97	2.59	0.81	2.10	2.87	0.64	2.34	2.86
Permeability model										
N (CV)	N (Pred.)	CV			Test			Prediction		
		R^2	MAE	RMSE	R^2	MAE	RMSE	R^2	MAE	RMSE
772	18	0.74	0.57	0.74	0.82	0.49	0.64	0.32	0.74	0.93

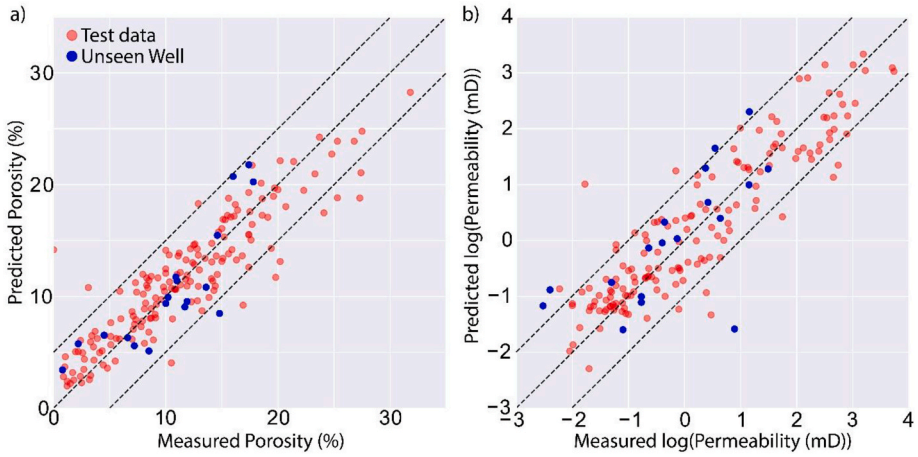

Fig. 14. Correlation of a) measured and predicted porosity and b) measured and predicted permeability for the single unseen well.

lower permeability values as compared to using the same measurement conditions, reducing the apparent model performance. Utilization of the same measurement protocols will likely result in more accurate model performance, as can be seen in the proof-of-concept study using a smaller curated dataset by Sadrikhanloo et al. (2026) (Table 2).

Furthermore, the utilization of different point-counting categories does not largely influence model predictions. As e.g., the presence of either pore-filling illite or undifferentiated pore-filling clay minerals both negatively affect permeability predictions, the model is able to capture the generally negative influence regardless of the assigned mineralogy during point-counting. However, to improve geological interpretability, future applications may still need to account for mineralogy- and texture-dependent influences on reservoir quality by increasing the specificity of mineral associations. Pore-lining illite at grain contacts have e.g., been shown to enhance pressure solution of quartz grains (Heald, 1955), whereas chlorite has not been described to have the same property, underlining the importance of mineral specific categorization. Additionally, non-standard petrographic categories (e.g., grain-coating coverages, Bloch et al. (2002)) and their quantification at different interfaces (Monsees et al., 2020; Busch et al., 2024, 2025), which show a decisive impact on porosity and permeability, are not captured by all presented datasets, and are therefore not included in the model. However, based on the results of the previous proof-of-concept study (Sadrikhanloo et al., 2026), they influence porosity and permeability predictions and could further enhance model performance.

The inclusion of grain size and sorting data is advised, as they can classically be related to differences in porosity and permeability (Beard and Weyl, 1973) and have been shown to influence previous machine learning models based on petrographic models (Sadrikhanloo et al., 2026). Including such features in future datasets could enhance predictive accuracy. While this may improve overall model performance, the performance just based on standard point-counting categories is already very promising.

Furthermore, enhancing machine learning-based machine vision classifications of mineral and rock types may help overcome another source of heterogeneity by limiting the effect of operator bias, if mineral textures are adequately differentiated. E.g., textures of clay mineral cements (i.e., pore-filling (radial or meshwork) or pore-lining (tangential)) matter for permeability (Neasham, 1977) and need to be accurately distinguished. However, previously outlined limitations in rock fragment classifications using machine vision (Tang et al., 2020) and the accurate discrimination of detrital grains and their syntaxial overgrowth cements have to be improved.

An advantage of the presented approach is the ability to evaluate detrital and authigenic controls on reservoir quality using SHAP values (Figs. 5 and 9), thereby increasing the understanding of reservoir systems and controlling factors on porosity and permeability. SHAP values highlight which petrographic features positively or negatively influence the target variables and can serve as a tool to interpret detrital, diagenetic, and compaction-related reservoir quality controls. Although these relationships are identified through data science applications, geological interpretation remains essential to uncover the underlying processes. This method can extend traditional workflows, which typically involve selective correlation of properties and rock typing analyses. During classical rock typing, specific mineral phases are related to porosity and permeability data. If only individual (typical) minerals and components, such as quartz and carbonate cements, and detrital matrix are considered, one may overlook critical reservoir quality controls. This may also uncover yet unknown correlations of petrographic properties with reservoir quality and enhance the data-driven evaluation and discovery of local reservoir quality controls, rather than relying on already published models. Using correlation matrix analysis or clustering analyses during rock typing may aid in defining relevant properties, but are not consistently specified to be used in published studies. This may be overcome by using data science applications, resulting in less biased studies on reservoir quality controls.

As machine learning models have been shown to effectively capture lithology- and location-specific relationships, this improved understanding could also enhance pre-drill predictions of reservoir quality. These insights could then be integrated into predictive reservoir quality models that account for the effects of pressure and temperature on compaction, cementation, and dissolution processes (e.g., Lander and Walderhaug, 1999; Walderhaug et al., 2000; Makowitz et al., 2006; Busch et al., 2018; Tamburelli et al., 2022).

3.9. *Possible future applications*

Geological datasets, including petrographic and core analysis data, are already available in most companies working in E&P and related industries or are (partly) publicly available in countries like e.g., the Netherlands and Norway (e.g., nlog or DISKOS). This can help create robust machine learning models to assess petrophysical properties. If a suitable calibration can be achieved, these models can potentially be applied to sample material from uncored wells, for which only cutting material is available. Cuttings are the only solid sample material produced at the surface during drilling of every well and they are, as standard, described at the well site to monitor drilling progress, and are partly kept for documentation purposes. As cuttings can be used to derive petrographic data, such as point-counting data (Radwan, 2022; Ölmez et al., 2025), they may potentially be used to gain predictions of porosity and permeability. This approach can potentially:

1) be used to gain porosity and permeability predictions for extended reservoir sections,
2) deliver predictions in cases, where the coring point was missed,
3) be used as a database for future subsurface utilization in sections above and below classical reservoir lithologies, all while
4) still delivering microstructural characterizations of detrital and diagenetic reservoir quality controls, which may not be possible just relying on well-log analysis.

Thereby, the information gained from sample material produced during drilling can be optimally utilized to gain reasonably accurate predictions solely based on petrographic input data. Especially in regions with high availability of geological data, the integration of porosity and permeability for uncored sections can enhance the modeling and predictive capabilities for e.g., geothermal utilization or CO_2 storage potential. Similar to re-evaluations of available core data in light of CO_2 storage (e.g., van Buggenum et al., 2025) this approach can fill gaps, where wells (and cuttings) are available but core material was not taken. The integration of cutting analyses may furthermore extend the information gain in well sections where, due to economic constraints or based on limited interest in certain sections of the stratigraphy, well log data was not acquired. Even in these sections, cuttings will be produced while drilling and are available for petrographic analyses.

As databases for cuttings already exist in some places (Norwegian Offshore Directorate, 2022), their value may already be maximized by utilizing machine learning. If a machine learning model is suitably calibrated to available core material capturing the range of effects of diagenetic alteration and compaction, it could be used to estimate likely porosity and permeability ranges based on point-counting analyses and data derived from these analyses. This may be especially valuable in scenarios, where due to slim economic margins (geothermal or brown-field extension) no core material is taken or where core was lost, and routine core analyses cannot be performed.

In light of e.g., the geothermal or storage utilization of sandstone lithologies (e.g., Heap et al., 2017; Underhill et al., 2023; Cheng et al., 2025), these methods may drastically improve the understanding of reservoir systems to target the most suitable reservoir sections. If properties like thermal conductivity, reservoir temperature, or other geophysical properties are included, economical assessments (e.g., Trainor-Guitton et al., 2025) for geothermal projects may be further supported by extended assessments of reservoir permeability.

When combined with well log-based machine learning approaches, the presented petrography-based machine learning approach can also be used to gain a better understanding on properties controlling reservoir-scale fluid flow and lead to more accurate reservoir models. In previous approaches petrography was only used to inform on sample textures and structures to aid the classification of well log-based petrofacies (Duarte et al., 2023). Utilizing the presented approach, the point-counted textures of e.g., clay minerals may extend such petrofacies classifications by also informing on flow properties of the captured rock- and mineral fabric obtained from thin sections.

Machine learning approaches in reservoir geology could be extended by including point-counting data and classical porosity and permeability analyses. They remain a highly flexible tool, which have already been successfully applied to well log data and simplified mineral mapping in petrographic samples. The presented datasets can likely be easily extended by other available data, as e.g., geochemical datasets (e.g., from XRF/pXRF/μXRF, EDX/S (e.g., Ölmez et al., 2025; Toth et al., 2025)) or mineralogical datasets (e.g., XRD, mineral mapping, (e.g., Busch et al., 2017b)) to address present and future questions relating to geological systems.

However, without sufficient core material, routine core analysis, and accurate state-of-the-art petrographic analyses for calibration datasets, predictions may become inaccurate due to incorrect assessment of controlling factors or local variations in diagenetic alteration. Accurate predictions of models like this require model calibration to authigenic and detrital phases showing an influence on petrophysical properties, emphasizing the need for geological understanding and calibration using core material.

4. Conclusion

1. The presented machine learning models show an overall very good predictive performance for both porosity ($R^2 = 0.87$, MAE = 1.77%, RMSE = 2.23%) and permeability ($R^2 = 0.82$, MAE = 0.47, RMSE = 0.64), with the latter considered acceptable due to the log-normal distribution of permeability values. These metrics remain consistent across four stratigraphic units (Upper Carboniferous, Permian Rotliegendes, Triassic Buntsandstein, and Jurassic sandstones) from 51 wells demonstrating that the models generalize well across different lithological sequences.
2. The models successfully incorporated mineral phases with limited occurrence (such as glauconite in Jurassic samples) demonstrating its ability to account for the mineralogical heterogeneity typical of diagenetically altered sedimentary rocks combining detrital material derived from different provenances. Even with data prepared by at least 21 different petrographers, performance decreases only slightly, suggesting limited operator bias as long as all point-count categories appear in the training dataset. Although curated datasets with unified point-counting categories and measurement protocols will likely yield slightly better performance, the presented approach remains effective despite the number of petrographers and differing or unspecified measurement conditions of petrophysical data.
3. Consistent cross-validation, test, and prediction metrics, also for unseen wells, implies model robustness. SHAP analyses reveal key petrographic controls on reservoir quality, and when interpreted geologically, provide a data-driven framework to understand how mineralogy and compaction influence porosity and permeability.
4. With calibration data from nearby wells, the models can potentially be used to estimate porosity and permeability from cuttings or chips when core material is unavailable, and they can be integrated with log-based machine learning workflows to enhance reservoir characterization.

CRediT authorship contribution statement

Benjamin Busch: Writing – original draft, Visualization, Methodology, Investigation, Formal analysis, Data curation, Conceptualization. **Christoph Hilgers:** Writing – review & editing, Conceptualization.

Declaration of competing interest

The authors declare that they have no known competing financial interests or personal relationships that could have appeared to influence the work reported in this paper.

Acknowledgements

BB and CH thankfully acknowledge previous provision of sample material for in-house studies by operators. We thankfully acknowledge the thorough and constructive review comments by two anonymous reviewers and editorial handling by Editor-in-Chief Hua Wang.

Appendix A. Supplementary data

Supplementary data to this article can be found online at https://doi.org/10.1016/j.aiig.2026.100202.

Data availability

All used research data is included in the supplementary data file.

References

Abdulkhaleq, H.B., Ibraheem, I.K., Al-Mudhafar, W.J., Mohammed, Z.T., Abd, M.S., 2025. Harnessing the power of machine learning for the optimization of CO2 sequestration in saline aquifers: applied on the tensleep formation at teapot dome in Wyoming. Geoenergy Sci. Eng. 245. https://doi.org/10.1016/j.geoen.2024.213522.

Adelmann, D., 2003. Sedimentology, Petrography and Reservoir Quality of Core 1 (Lower Germanic Triassic) (Part I) and Petrography and Reservoir Quality of Sidewall Samples (Part II) of Well F16-4. PanTerra Geoconsultants B.V., p. 141

Adelmann, D., 2004. Sedimentology, Petrography and Reservoir Quality of Cores 1 and 2 (Lower Slochteren Sandstone) in Well L5-10 and Petrography of Cutting Samples from the Carboniferous in Well L5-10. PanTerra Geoconsultants, Leiderdorp, The Netherlands, p. 124.

Ajdukiewicz, J.M., Lander, R.H., 2010. Sandstone reservoir quality prediction: the state of the art. AAPG (Am. Assoc. Pet. Geol.) Bull. 94 (8), 1083–1091. https://doi.org/10.1306/intro060110.

Anderson, C., Innes, B., Smith, E., 2000. Routine Core Analysis & Petrography of 15 Triassic Sidewall Cores (Volpriehausen Sandstone & Lower Buntsandstein). Core Laboratories, (U.K.), Aberdeen, Scotland, p. 38.

Baunack, C., 2005. Sedimentology, Petrography and Reservoir Quality of the Early Triassic Deposits in Well Q4-C2. PanTerra Geoconsultants B.V, Leiderdorp, The Netherlands, p. 119.

Beard, D.C., Weyl, P.K., 1973. Influence of texture on porosity and permeability of unconsolidated sand. AAPG (Am. Assoc. Pet. Geol.) Bull. 57 (2), 349–369.

Bentéjac, C., Csörgő, A., Martínez-Muñoz, G., 2020. A comparative analysis of gradient boosting algorithms. Artif. Intell. Rev. 54 (3), 1937–1967. https://doi.org/10.1007/s10462-020-09896-5.

Bergen, K.J., Johnson, P.A., de Hoop, M.V., Beroza, G.C., 2019. Machine learning for data-driven discovery in solid Earth geoscience. Science 363, 6433. https://doi.org/10.1126/science.aau0323.

Bloch, S., Lander, R.H., Bonnell, L.M., 2002. Anomalously high porosity and permeability in deeply buried sandstone reservoirs: origin and predictability. AAPG (Am. Assoc. Pet. Geol.) Bull. 86, 301–328. https://doi.org/10.1306/61EEDABC-173E-11D7-8645000102C1865D.

Boels, J., 2003. Sedimentology, Petrography and Reservoir Quality of the Upper Carboniferous in Well E10-3. PanTerra Geoconsultants B.V, Leiderdorp, The Netherlands, p. 97.

Boels, J., Nortier, J.W., 2004. Sedimentology, Petrography and Reservoir Quality of Core 1 of Well F16-5. PanTerra Geoconsultants B.V, Leiderdorp, The Netherlands, p. 87.

Burfoot, W., Matheson, F., Phillips, I., Elphinstone, J., 2002a. An Integrated Geological & Petrophysical Investigation of Triassic Volpriehausen Core from Well G17cd-A2 (Offshore Netherlands). Core Laboratories, U.K.) Limited, Aberdeen, Scotland, p. 90.

Burfoot, W., Matheson, F., Phillips, I., Rushton, J., Elphinstone, J., 2004. An Integrated Geological & Petrophysical Investigation of Triassic Volpriehausen Core from Well G14-3 (Offshore Netherlands). Core Laboratories (U.K.) Limited, Aberdeen, Scotland, p. 105.

Burfoot, W., Mueller, S., Pauley, C., Deadman, S., 2009. An Integrated Geological and Petrophysical Investigation of Triassic Core from Well G14-B2 (Offshore Netherlands). Core Laboratories (U.K.) Limited, Aberdeen, Scotland, p. 103.

Burfoot, W., Mueller, S., Rushton, J., Elphinstone, J., 2005. An Integrated Geological & Petrophysical Investigation of Triassic Dethfurth Sandstone & Volpriehausen Claystone Core from Well G14-4 (Offshore Netherlands). Core Laboratories (U.K.) Limited, Aberdeen, Scotland.

Burfoot, W., Wood, J., Matheson, F., Cook, G., Elphinstone, J., 2002b. An Integrated Geological & Petrophysical Investigation of Permian Rotliegend Core from Well K12-16 (Offshore Netherlands). Core Laboratories, U.K.) Limited, Aberdeen, Scotland, p. 21.

Busch, A., Schweinar, K., Kampman, N., Coorn, A., Pipich, V., Feoktystov, A., Leu, L., Amann-Hildenbrand, A., Bertier, P., 2017a. Determining the porosity of mudrocks using methodological pluralism. Geol. Soc. London Spec. Publ. 454 (1), 15–38. https://doi.org/10.1144/sp454.1.

Busch, B., Adelmann, D., Herrmann, R., Hilgers, C., 2022. Controls on compactional behavior and reservoir quality in a Triassic Buntsandstein reservoir, upper rhine graben, SW Germany. Mar. Petrol. Geol. 136, 105437. https://doi.org/10.1016/j.marpetgeo.2021.105437.

Busch, B., Becker, I., Koehrer, B., Adelmann, D., Hilgers, C., 2019. Porosity evolution of two upper Carboniferous tight-gas-fluvial sandstone reservoirs: impact of fractures and total cement volumes on reservoir quality. Mar. Petrol. Geol. 100, 376–390. https://doi.org/10.1016/j.marpetgeo.2018.10.051.

Busch, B., Böcker, J., Hilgers, C., 2024. Improved reservoir quality assessment by evaluating illite grain coatings, quartz cementation, and compaction – case study from the Buntsandstein, upper rhine graben. Germany Geoenerg. Sci. Eng. 241, 213141. https://doi.org/10.1016/j.geoen.2024.213141.

Busch, B., Böke, L.L., Schmidt, C., Warnecke, M., Hilgers, C., 2025. Reservoir quality controls in the lower buntsandstein and their relation to detrital grain size, URG, SW-Germany. Geothermics 132, 103453. https://doi.org/10.1016/j.geothermics.2025.103453.

Busch, B., Hilgers, C., Gronen, L., Adelmann, D., 2017b. Cementation and structural diagenesis of fluvio-aeolian rotliegend sandstones, northern England. J. Geol. Soc. 174, 855–868. https://doi.org/10.1144/jgs2016-122.

Busch, B., Hilgers, C., Lander, R.H., Bonnell, L.M., Adelmann, D., 2018. Reservoir quality and burial model evaluation by kinetic quartz and illite cementation modeling: case study Rotliegendes, N-Germany. AAPG (Am. Assoc. Pet. Geol.) Bull. 101 (2), 293–307. https://doi.org/10.1306/0503171605217075.

Cater, J.M.L., 2001a. Sedimentology, Petrography and Reservoir Quality of Core 1 (Lower Slochteren and Westphalian D) in Well F16-03. PanTerra Geoconsultants B.V., p. 108

Cater, J.M.L., 2001b. Sedimentology, Petrography and Reservoir Quality of Core 1 (Lower Slochteren Sandstone) in Well E18-04. PanTerra Geoconsultants B.V, Warmond, The Netherlands, p. 99.

Cater, J.M.L., 2001c. Sedimentology, Petrography and Reservoir Quality of Core 1 (Upper Slochteren Sandstone) in Well L10-M2. PanTerra Geoconsultants B.V., Leiderdorp, The Netherlands, p. 80.

Chen, Y., Tang, S., Xi, Z., Sun, S., Wang, J., Lin, D.K.Z., Mei, X., 2025. Predicting geomechanical properties of heterogeneous shale using ensemble learning methods. Geoenergy Sci. Eng. 256, 214148. https://doi.org/10.1016/j.geoen.2025.214148.

Cheng, C., Busch, B., Kontny, A., Hilgers, C., 2025. Underground hydrogen storage in sandstone reservoirs: effects of geochemical reactivity of hydrogen on reservoir performance. Int. J. Hydrogen Energy 105, 492–504. https://doi.org/10.1016/j.ijhydene.2025.01.330.

Dalhat, M.A., Osman, S.A., 2025. Deep learning based identification of rock minerals from un-processed digital microscopic images of undisturbed broken-surfaces. Artif. Intell. Geosci. 6, 100127. https://doi.org/10.1016/j.aiig.2025.100127.

David, C., Wong, T.-f., Zhu, W., Zhang, J., 1994. Laboratory measurement of compaction-induced permeability change in porous rocks: implications for the generation and maintenance of pore pressure excess in the crust. Pure Appl. Geophys. 143 (1/2/3), 425–456. https://doi.org/10.1007/BF00874337.

Dramsch, J.S., 2020. 70 years of machine learning in geoscience in review. In: Machine Learning in Geosciences, pp. 1–55. https://doi.org/10.1016/bs.agph.2020.08.002.

Du, Z., Xu, L., Yin, S., Dong, S., Dai, Z., Ma, Y., Thanh, H.V., Soltanian, M.R., 2025. Enhanced prediction and uncertainty analysis for hydrogen production rate in depleted oil and gas reservoirs using advanced machine learning techniques. Geoenergy Sci. Eng. 249. https://doi.org/10.1016/j.geoen.2025.213795.

Duarte, D., Pires de Lima, R., Tellez, J., Pranter, M.J., 2023. Spatial variability of petrofacies using supervised machine learning and geostatistical modeling: Sycamore formation, Sho-Vel-Tum field, Oklahoma, USA. Interpretation 11 (2), T289–T302. https://doi.org/10.1190/int-2022-0064.1.

Dubois, M.K., Bohling, G.C., Chakrabarti, S., 2007. Comparison of four approaches to a rock facies classification problem. Comput. Geosci. 33 (5), 599–617. https://doi.org/10.1016/j.cageo.2006.08.011.

Esmaeili, B., Hosseinzadeh, S., Kadkhodaie, A., Wood, D.A., Akbarzadeh, S., 2024. Simulating reservoir capillary pressure curves using image processing and classification machine learning algorithms applied to petrographic thin sections. J. Afr. Earth Sci. 209. https://doi.org/10.1016/j.jafrearsci.2023.105098.

Faria, E.L., Barbosa, R., Coelho, J.M., Matos, T.F., Santos, B.C.C., Gonzalez, J.L., Bom, C. R., de Albuquerque, M.P., Russano, P.J., de Albuquerque, M.P., 2025. Automatic classification of carbonatic thin sections by computer vision techniques and one-vs-all models. Artif. Intell. Geosci. 6, 1. https://doi.org/10.1016/j.aiig.2025.100117.

Felder, M., 2009. Petrography and Reservoir Quality of Lower Slochteren and Carboniferous Rotary Sidewall Cores from Well E16-4. Dutch Offshore. PanTerra Geoconsultants B.V, Leiderdorp, The Netherlands, p. 75.

Felder, M., 2010a. Sedimentology, Petrography and Reservoir Quality of Rotliegend Deposits in Well L5-11. PanTerra Geoconsultants B.V., Leiderdorp, The Netherlands, p. 82.

Felder, M., 2010b. Sedimentology, Petrography and Reservoir Quality of Volpriehausen Sandstones in Well M01-04. PanTerra Geoconsultants B.V., Leiderdorp, The Netherlands, p. 70.

Felder, M., 2013. Assessment of Controls on Reservoir Quality for 3 Wells in the K18 Block. PanTerra Geoconsultants B.V, Leiderdorp, The Netherlands, p. 85.

Felder, M., Kneen, R.D., Petrea, C., 2016. Sedimentology, Petrography and Reservoir Quality of Core 1 from Well M07-10, Offshore the Netherlands. PanTerra Geoconsultants B.V, Leiderdorp, The Netherlands, p. 167.

Felder, M., Pierau, R., 2010a. Petrography and Reservoir Quality of Rotary Sidewall Cores from Well E17a A3. PanTerra Geoconsultants B.V, Leiderdorp, The Netherlands, p. 65.

Felder, M., Pierau, R., 2010b. Sedimentology, Petrography and Reservoir Properties of Upper Slochteren Sandstones from Well L11b-A06 (Renamed from L11-13), Rotliegendes, Dutch Offshore. PanTerra Geoconsultants B.V, Leiderdorp, The Netherlands, p. 95.

Felder, M., Pierau, R., 2013. Integrated Study of Sedimentological and Petrographical Properties of the Rotliegend Interval of Wells L06-07 and L06-08, Dutch Offshore. PanTerra Geoconsultants B.V, Leiderdorp, The Netherlands, p. 43.

Folk, R.L., 1980. Petrology of Sedimentary Rocks. Hemphill Publishing Company, Austin, Texas, U.S.A., p. 182

Guo, Z., Sankaran, S., 2025. Hybrid RGNet: a physics-based model enhanced by machine learning for history matching, characterization and future prediction. Geoenergy Sci. Eng. 246. https://doi.org/10.1016/j.geoen.2024.213597.

Guryanov, A., 2019. Histogram-based algorithm for building gradient boosting ensembles of piecewise linear decision trees. In: van der Aalst, W.M.P., batagelj, V., Ignatov, D.I., Khachay, M., Kuskova, V., Kutuzov, A., Knuznetsov, S.O., Lomazova, I. A., Loukachevitch, N., Napoli, A., Pardalos, P.M., Pelillo, M., Savchenko, A.V., Tutubalina, E. (Eds.), Analysis of Images, Social Networks and Texts. Springer, Chan, SUI, pp. 39–50. https://doi.org/10.1007/978-3-030-37334-4_4.

Heald, M.T., 1955. Stylolites in sandstone. J. Geol. 63, 101–114. https://doi.org/10.1086/626237.

Heap, M.J., Kushnir, A.R.L., Gilg, H.A., Wadsworth, F.B., Reuschlé, T., Baud, P., 2017. Microstructural and petrophysical properties of the permo-triassic sandstones (Buntsandstein) from the Soultz-sous-Forêts geothermal site (France). Geoth. Energy 5, 1. https://doi.org/10.1186/s40517-017-0085-9.

Houseknecht, D.W., 1987. Assessing the relative importance of compaction processes and cementation to reduction of porosity in sandstones. AAPG (Am. Assoc. Pet. Geol.) Bull. 71, 633–642.
Hurst, A., Nadeau, P.H., 1995. Clay microporosity in reservoir sandstones: an application of quantitative electron microscopy in petrophysical evaluation. AAPG (Am. Assoc. Pet. Geol.) Bull. 79 (4), 563–573.
John, T., 2005. Sedimentology, Petrography and Reservoir Quality of Cores 1-3 of Well L8-16x. PanTerra Geoconsultants B.V, Leiderdorp, The Netherlands, p. 157.
John, T., 2006. Sedimentology, Petrography and Reservoir Quality of Core 1 of Well D12-A2. PanTerra Geoconsultants B.V, Leiderdorp, The Netherlands, p. 109.
John, T., Baunack, C., 2006. Sedimentology, Petrography and Reservoir Quality of the Cored Interval of Well F16-A3. PanTerra Geoconsultants B.V, Leiderdorp, The Netherlands, p. 112.
Johnson, J.I., Sharman, G.R., Szymanski, E., Huang, X., 2022. Machine learning applied to a modern-pleistocene petrographic data set: the global prediction of sand modal composition (GloPrSM) model. J. Geophys. Res.: Earth Surf. 127 (7). https://doi.org/10.1029/2022jf006595.
Joshua, P., Marquis, G., Maurer, V., Glaas, C., Montagud, A., Formento, J.L., Genter, A., Darnet, M., 2024. Rock mineral volume inversion using statistical and machine learning algorithms for Enhanced geothermal systems in upper rhine graben, Eastern France. J. Geophys. Res.: Mach. Learn. Computat. 1, 2. https://doi.org/10.1029/2024jh000154.
Karpatne, A., Ebert-Uphoff, I., Ravela, S., Babaie, H.A., Kumar, V., 2019. Machine learning for the geosciences: challenges and opportunities. IEEE Trans. Knowl. Data Eng. 31 (8), 1544–1554. https://doi.org/10.1109/tkde.2018.2861006.
Klinkenberg, L.J., 1941. The Permeability of Porous Media to Liquids and Gases, Drilling and Production Practice. American Petroleum Institute, New York.
Kneen, R.D., Petrea, C., 2015. Sedimentology, Petrography and Reservoir Quality of Cores 1 - 2 from Well M07-08, Offshore the Netherlands. PanTerra Geoconsultants B.V, Leiderdorp, The Netherlands, p. 234.
Kristiansen, K., Valtiner, M., Greene, G.W., Boles, J.R., Israelachvili, J.N., 2011. Pressure solution - the importance of the electrochemical surface potential. Geochem. Cosmochim. Acta 75, 6882–6892. https://doi.org/10.1016/j.gca.2011.09.019.
Lander, R.H., Walderhaug, O., 1999. Predicting porosity through simulating sandstone compaction and quartz cementation. AAPG (Am. Assoc. Pet. Geol.) Bull. 83 (3), 433–449. https://doi.org/10.1306/00AA9BC4-1730-11D7-8645000102C1865D.
Lanson, B., Beaufort, D., Berger, G., Bauer, A., Cassagnabère, A., Meunier, A., 2002. Authigenic kaolin and illitic minerals during burial diagenesis of sandstones: a review. Clay Miner. 37 (1), 1–22. https://doi.org/10.1180/0009855023710014.
Lundberg, S.M., Lee, S.-I., 2017. A unified approach to interpreting model predictions. In: von Luxburg, U., Guyon, I., Bengio, S., Wallach, H., Fergus, R. (Eds.), NIPS'17: Proceedings of the 31st International Conference on Neural Information Processing Systems. Curran Associates Inc., Red Hook, NY, USA, Long Beach, CA, USA, pp. 4768–4777.
Lv, P., Chen, W., Zou, X., 2025. Precision recognition of rock thin section images with multi-head self-attention convolutional neural networks. J. Geophys. Res.: Mach. Learn. Computat. 2, 2. https://doi.org/10.1029/2025jh000617.
Makowitz, A., Lander, R.H., Milliken, K.L., 2006. Diagenetic modeling to assess the relative timing of quartz cementation and brittle grain processes during compaction. AAPG (Am. Assoc. Pet. Geol.) Bull. 90 (6), 873–885. https://doi.org/10.1306/12190505044.
Male, F., Duncan, I.J., 2020. Lessons for machine learning from the analysis of porosity-permeability transforms for carbonate reservoirs. J. Petrol. Sci. Eng. 187. https://doi.org/10.1016/j.petrol.2019.106825.
Meier, A., Felder, M., Zhang, X., 2014. Sedimentology, Petrography and Reservoir Quality of Well P06-A7. PanTerra Geoconsultants B.V, Leiderdorp, The Netherlands, p. 150.
Mendoza, J.D.S., Felder, M., 2010a. Sedimentology, Petrography and Reservoir Quality of the Early Triassic Deposits in Well Q1-27. PanTerre Geoconsultants B.V., Leiderdorp, The Netherlands, p. 168.
Mendoza, J.D.S., Felder, M., 2010b. Sedimentology, Petrography and Reservoir Quality of the Early Triassic Deposits in Well Q1-28. PanTerra Geoconsultants B.V., Leiderdorp, The Netherlands, p. 165.
Mishra, A., Sharma, A., Patidar, A.K., 2022. Evaluation and development of a predictive model for geophysical well log data analysis and reservoir characterization: machine learning applications to lithology prediction. Nat. Resour. Res. 31 (6), 3195–3222. https://doi.org/10.1007/s11053-022-10121-z.
Monsees, A.C., Busch, B., Schöner, N., Hilgers, C., 2020. Rock typing of diagenetically induced heterogeneities – a case study from a deeply-buried clastic Rotliegend reservoir of the Northern German basin. Mar. Petrol. Geol. 113, 104163. https://doi.org/10.1016/j.marpetgeo.2019.104163.
Morano, S., Ogundu, M., Chambers, C., 2007. Petrographic Report - De Ruyter Exploration Wells - Well P11-05. Corex (UK) Ltd, Aberdeen, Scotland, p. 76.
Neasham, J.W., 1977. The morphology of dispersed clay in sandstone reservoirs and its effect on sandstone shaliness, pore space and fluid flow properties. In: SPE Annual Fall Technical Conference and Exhibition. Denver, CO.
Nhat-Duc, H., Van-Duc, T., 2023. Comparison of histogram-based gradient boosting classification machine, random Forest, and deep convolutional neural network for pavement raveling severity classification. Autom. ConStruct. 148. https://doi.org/10.1016/j.autcon.2023.104767.
Nortier, J.W., 2005. Sedimentology, Petrography and Reservoir Quality of Cores 1-3 of Well L6-6. PanTerra Geoconsultants B.V, Leiderdorp, The Netherlands, p. 124.
Nortier, J.W., 2007. Sedimentology, Petrography and Reservoir Quality of Core 1 and Core 2 (Upper Jurassic Aerdenhout Member) in Well K18-Kotter-14. PanTerra Geoconsultants B.V, Leiderdorp, The Netherlands, p. 106.
Nortier, J.W., Baunack, C., Juhasz-Bodnar, K., 2005. Sedimentology, Petrography and Reservoir Quality of Cores 1-4 of Well K18-7X and Petrography of Sidewall Samples from Well K18-7. PanTerra Geoconsultants B.V, Leiderdorp, The Netherlands, p. 265.
Nortier, J.W., Boels, J., 2005. Sedimentology, Petrography and Reservoir Properties of Scruff Sandstone and Carbonate Breccia in Core 1, Well G16a-A1 and Petrography of Sidewall Samples from Sidetrack Well G16a-A1st. PanTerra Geoconsultants B.V, Leiderdorp, The Netherlands, p. 127.
Norwegian Offshore Directorate, 2022. In: NOROG Digital Cuttings Project. https://www.sodir.no/en/diskos/wells/historical-projects/norog-digital-cuttings-project/.
Ölmez, J.A., Busch, B., Möbius, R., Dasgupta, K., Gauer, A., Tosoratti, F., Hilgers, C., 2025. Reservoir characterization and well production proxy analyses on drill cuttings: case study from the flysch play in the Vienna basin (NE Austria). Energy Geosci. 6, 100461. https://doi.org/10.1016/j.engeos.2025.100461.
Ore, T., Gao, D., 2023. Prediction of reservoir brittleness from geophysical logs using machine learning algorithms. Comput. Geosci. 171. https://doi.org/10.1016/j.cageo.2022.105266.
Orlander, T., Milsch, H., Fabricius, I.L., 2021. Comparison of gas, Klinkenberg, and liquid permeability of sandstone: flow regime and pore size. AAPG (Am. Assoc. Pet. Geol.) Bull. 105 (7), 1383–1403. https://doi.org/10.1306/12222019138.
Paucar, S., Mejia-Escobar, C., Collaguazo, V., 2025. Automatic description of rock thin sections: a web application. Artif. Intell. Geosci. 6, 1. https://doi.org/10.1016/j.aiig.2025.100118.
Paxton, S.T., Szabo, J.O., Ajdukiewicz, J.M., Klimentidis, R.E., 2002. Construction of an intergranular compaction curve for evaluating and predicting compaction and porosity loss in rigid grain sandstone reservoirs. AAPG (Am. Assoc. Pet. Geol.) Bull. 86 (12), 2047–2067. https://doi.org/10.1306/61EEDDFA-173E-11D7-8645000102C1865D.
Petrea, C., Goldberg, T., 2013. Sedimentology, Petrography and Reservoir Quality of Core and Sidewall Samples from Well K18-9. PanTerra Geoconsultants B.V, Leiderdorp, The Netherlands, p. 206.
Petrea, C., Meier, A., 2014. Sedimentology, Petrography and Reservoir Quality of the Cored Interval (Hardegsen Formation - Triassic Buntsandstein) of Well P11-11, Dutch Offshore. PanTerra Geoconsultants B.V, Leiderdorp, The Netherlands, p. 95.
Pinheiro, J.M.H., de Oliveira, S.V.B., Silva, T.H.S., Saraiva, P.A.R., de Souza, E.F., Ambrosio, L.A., Becker, M., 2025. The Impact of Feature Scaling in Machine Learning: Effects on Regression and Classification Tasks.
Radwan, A.E., 2022. Provenance, depositional facies, and diagenesis controls on reservoir characteristics of the middle Miocene tidal sandstones, Gulf of Suez rift basin: integration of petrographic analysis and gamma-ray log patterns. Environ. Earth Sci. 81 (15). https://doi.org/10.1007/s12665-022-10502-w.
Ransinangue, A., Labourdette, R., Houzay, E., Guillon, S., Bourillot, R., Dujoncquoy, E., Chehata, N., 2025. SynSection: Sedimentology-driven data generation for deep learning applications in carbonates petrography. Mar. Petrol. Geol. 182. https://doi.org/10.1016/j.marpetgeo.2025.107490.
RedRock Associates International Limited, 2007. A Study of the Sedimentology and Petrography of Volpriehausen Formation Core from Well P10-05, Southern North Sea, Offhore Netherlands. RedRock Associates International Limited, Geological Consultants, p. 115.
Rider, M., Kennedy, M., 2011. The Geological Interpretation of Well Logs, 3 ed. Rider-French Consulting Ltd, Scotland.
Rieckmann, M., 1970. Untersuchung von Turbulenzerscheinungen beim Fließen von Gasen durch Speichergesteine unter Berücksichtigung der Gleitströmung. Erdoel-Erdgas-Zeitschrift 86, 36–51.
Rieke, H., 2003. Sedimentology, Petrography and Reservoir Quality of Cores 1 to 6 (Lower Slochteren Sandstone and Carboniferous) in Well L5-9. PanTerra Geoconsultants B.V, Leiderdorp, The Netherlands, p. 142.
Rubo, R.A., de Carvalho Carneiro, C., Michelon, M.F., Gioria, R.d.S., 2019. Digital petrography: mineralogy and porosity identification using machine learning algorithms in petrographic thin section images. J. Petrol. Sci. Eng. 183. https://doi.org/10.1016/j.petrol.2019.106382.
Sadlok, G., Mueller, S., Matheson, F., 2014. Geological Investigation of Core from Well L5-15 (Offshore Netherlands). Core Laboratories (U.K.) Ltd, Aberdeen, Scotland, p. 75.
Sadrikhanloo, S., Busch, B., Hilgers, C., 2026. Porosity and permeability prediction from petrographic point-counting data using machine learning: applications to Rotliegendes and Buntsandstein reservoirs. Energy Geosci 7, 100537. https://doi.org/10.1016/j.engeos.2026.100537.
Saxena, N., Day-Stirrat, R.J., Hows, A., Hofmann, R., 2021. Application of deep learning for semantic segmentation of sandstone thin sections. Comput. Geosci. 152. https://doi.org/10.1016/j.cageo.2021.104778.
Schaefer, H.-J., Rehfeld-Kiefer, U., Docherty, S., 2008. Plug Description and Petrographic Reservoir Geology Study. Corex (UK) Ltd, Aberdeen, Scotland, p. 130.
Shahani, N.M., Kamran, M., Zheng, X., Liu, C., Guo, X., Ye, Z., 2021. Application of gradient boosting machine learning algorithms to predict uniaxial compressive strength of soft sedimentary rocks at thar coalfield. Adv. Civ. Eng. 1. https://doi.org/10.1155/2021/2565488, 2021.
Shi, F., Liao, H., Wang, S., Alfarisi, O., Qu, F., 2025. Optimization of drilling rate based on genetic algorithms and machine learning models. Geoenergy Sci. Eng. 247. https://doi.org/10.1016/j.geoen.2025.213747.
Sinha, U., Dindoruk, B., 2025. Review of physics-informed machine learning (PIML) methods applications in reservoir engineering. Geoenergy Sci. Eng. https://doi.org/10.1016/j.geoen.2025.213713.
Soromotin, A.V., Martyushev, D.A., Junho Pereira, J.L., 2025. On the application of machine learning algorithms in predicting the permeability of oil reservoirs. Artif. Intell. Geosci. 6, 2. https://doi.org/10.1016/j.aiig.2025.100126.

Storvoll, V., Bjørlykke, K., Karlsen, D., Saigal, G., 2002. Porosity preservation in reservoir sandstones due to grain-coating illite: a study of the Jurassic garn formation from the kristin and lavrans fields, offshore mid-Norway. Mar. Petrol. Geol. 19, 767–781. https://doi.org/10.1016/S0264-8172(02)00035-1.

Sun, J., Zhang, R., Chen, M., Chen, B., Wang, X., Li, Q., Ren, L., 2021. Identification of porosity and permeability while drilling based on machine learning. Arabian J. Sci. Eng. 46 (7), 7031–7045. https://doi.org/10.1007/s13369-021-05432-x.

Tamburelli, S., Di Giulio, A., Amadori, C., Consonni, A., Ortenzi, A., 2022. New constraint on burial and thermal history of Devonian reservoir sandstones in the Illizi-Ghadames basin (North Africa) through diagenetic numerical modelling. Mar. Petrol. Geol. 145. https://doi.org/10.1016/j.marpetgeo.2022.105903.

Tang, D.G., Milliken, K.L., Spikes, K.T., 2020. Machine learning for point counting and segmentation of arenite in thin section. Mar. Petrol. Geol. 120. https://doi.org/10.1016/j.marpetgeo.2020.104518.

Thomas, W.H., Ringen, J.K., Rasch, S.O., 2003. Effect of Glauconite on Petrophysical Properties as Revealed by Core Analysis. International Symposium of the Society of Core Analysts, Pau, France, p. 12.

Toth, N., Shi, S., Maclennan, J., Tung, P.Y., 2025. EDS analysis for petrology: a probabilistic framework with GPyEDS. J. Geophys. Res.: Mach. Learn. Computat. 2, 4. https://doi.org/10.1029/2025jh000751.

Trainor-Guitton, W., Menon, K., Pinchuk, P., Thomson, S.M., Hart-Wagoner, N., Lu, C., Mlawsky, E., Coolbaugh, M., Lindsey, C., Faulds, J., 2025. "Hidden" hydrothermal technical potential & technoeconomics: revealing permeability & fluids with more data. Geothermics 133. https://doi.org/10.1016/j.geothermics.2025.103473.

Underhill, J.R., de Jonge-Anderson, I., Hollinsworth, A.D., Fyfe, L.C., 2023. Use of exploration methods to repurpose and extend the life of a super basin as a carbon storage hub for the energy transition. AAPG (Am. Assoc. Pet. Geol.) Bull. 107 (8), 1419–1474. https://doi.org/10.1306/04042322097.

van Buggenum, J.M., Davids, B., Ravestein, T., 2025. A Map-based Analysis of the Theoretical CO_2 Storage Capacity in the Rotliegend Aquifer of the Dutch Offshore. TNO Public. TNO, p. 77.

van Dijk, C.P.J., 2003. Sedimentology, Petrography and Reservoir Properties of Friese Front and Scruff Greensand in Cores 1 and 2, Well G16-6A. PanTerra Geoconsultants B.V, Leiderdorp, The Netherlands, p. 55.

Walderhaug, O., Lander, R.H., Bjørkum, P.A., Oelkers, H., Bjørlykke, K., Nadeau, P.H., 2000. Modelling quartz cementation and porosity in reservoir sandstones: examples from the Norwegian continental shelf. In: Worden, R.H., Morad, S. (Eds.), Quartz Cementation in Sandstones. Blackwell Science Ltd., Oxford, pp. 39–49. https://doi.org/10.1002/9781444304237.ch3.

Wood, D.A., 2020. Predicting porosity, permeability and water saturation applying an optimized nearest-neighbour, machine-learning and data-mining network of well-log data. J. Petrol. Sci. Eng. 184. https://doi.org/10.1016/j.petrol.2019.106587.

Worden, R.H., Armitage, P.J., Butcher, A.R., Churchill, J.M., Csoma, A.E., Hollis, C., Lander, R.H., Omma, J.E., 2018. Petroleum reservoir quality prediction: overview and contrasting approaches from sandstone and carbonate communities. In: Armitage, P.J., Butcher, A.R., Churchill, J.M., Csoma, A.E., Hollis, C., Lander, R.H., Omma, J.E., Worden, R.H. (Eds.), Reservoir Quality of Clastic and Carbonate Rocks: Analysis, Modelling and Prediction. Geological Society, London, pp. 1–31. https://doi.org/10.1144/SP435.21.

Wrona, T., Pan, I., Gawthorpe, R.L., Fossen, H., 2018. Seismic facies analysis using machine learning. Geophysics 83 (5), O83–O95. https://doi.org/10.1190/geo2017-0595.1.

Xia, L., Zheng, P., Li, J., Huang, X., Gao, R.X., 2024. Histogram-based gradient boosting tree: a federated learning approach for collaborative fault diagnosis. IEEE ASME Trans. Mechatron. 29 (4), 2637–2648. https://doi.org/10.1109/tmech.2023.3331712.

Yang, T., Tang, H., Dai, J., Wang, H., Wen, X., Wang, M., He, J., Wang, M., 2025. Quantitative classification and prediction of pore structure in low porosity and low permeability sandstone: a machine learning approach. Geoenergy Sci. Eng. 247. https://doi.org/10.1016/j.geoen.2025.213708.

Yu, J., Wellmann, F., Virgo, S., von Domarus, M., Jiang, M., Schmatz, J., Leibe, B., 2023. Superpixel segmentations for thin sections: evaluation of methods to enable the generation of machine learning training data sets. Comput. Geosci. 170. https://doi.org/10.1016/j.cageo.2022.105232.